Pan-cancer prediction of tumor immune activation and response to immune checkpoint blockade from tumor transcriptomics and histopathology

Sumit Mukherjee[1,*], Sumeet Patiyal[1,*], Lipika R. Pal[1], Tian-Gen Chang[1], Sumona Biswas[1], Saugato Rahman Dhruba[1], Amos Stemmer[1], Arashdeep Singh[1], Abbas Yousefi-Rad[2], Tien-Hua Chen[3], Binbin Wang[1], Denis Marino[4], Wonwoo Shon[5], Yuan Yuan[5], Mark Faries[5], Omid Hamid[5], Karen Reckamp[5], Barliz Waissengrin[5], Beatriz Ornelas[5], Pen-Yuan Chu[6], Salah Boudjadi[2], Lisa Ley[2], Dilara Akbulut[2], Nourhan El Ahmar[7,8], Sabina Signoretti[7,8,9,10], David A. Braun[11], Hyunjeong Joo[12], Hyungsoo Kim[12], Arsen Osipov[4], Robert A. Figlin[4], Jair Bar[13], Iris Barshack[13], Chi-Ping Day[1], Karine Sargsyan[3,14], Andrea B. Apolo[2], Kenneth Aldape[15], Muh-Hwa Yang[16], Michael B. Atkins[17], Ze'ev A. Ronai[12,✉], Danh-Tai Hoang[1,✉], Eytan Ruppin[1,✉]

[1]Cancer Data Science Laboratory, Center for Cancer Research, National Cancer Institute, National Institutes of Health, Bethesda, MD, USA.
[2]Genitourinary Malignancies Branch, Center for Cancer Research, National Cancer Institute, National Institutes of Health, Bethesda, MD, USA.
[3]School of Medicine, National Yang Ming Chiao Tung University, Taiwan.
[4]OncoBiobank, Cancer Center, Cedars-Sinai Medical Center, Los Angeles, CA, USA.
[5]Cedars-Sinai Medical Center, Los Angeles, CA, USA.
[6]Department of Otolaryngology, Taipei Veterans General Hospital, Taipei, Taiwan.
[7]Department of Pathology, Brigham and Women's Hospital, Boston, MA, USA.
[8]Harvard Medical School, Boston, MA, USA.
[9]Broad Institute, Cambridge, MA, USA.
[10]Department of Oncologic Pathology, Dana-Farber Cancer Institute, Boston, MA, USA.
[11]Center of Molecular and Cellular Oncology, Yale Cancer Center, Yale School of Medicine, New Haven, CT, USA.
[12]Jim and Eleanor Randall Department of Surgery and the Department of Biomedical Sciences, Cedars-Sinai Medical Center, Los Angeles, CA, USA.
[13]Department of Pathology, Sheba Medical Center, Ramat Gan, Israel.
[14]International Biobanking, Medical University of Graz, Austria
[15]Laboratory of Pathology, Center for Cancer Research, National Cancer Institute, National Institutes of Health, Bethesda, MD, USA.
[16]Institute of Clinical Medicine, National Yang Ming Chiao Tung University, Taipei, Taiwan.
[17]Georgetown Lombardi Comprehensive Cancer Center, Washington, DC, USA.

[*] Equally contributing first authors: Sumit Mukherjee, Sumeet Patiyal

✉ Corresponding authors: Zeev.Ronai@cshs.org, danh-tai.hoang@nih.gov, eytan.ruppin@nih.gov

Abstract

Accurately predicting which patients will respond to immune checkpoint blockade (ICB) remains a major challenge. Here, we present TIME_ACT, an unsupervised 66-gene transcriptomic signature of tumor immune activation derived from TCGA melanoma data. First, TIME_ACT scores accurately identify tumors with activated immune microenvironments across cancer types. Analysis of spatial features of the tumor microenvironment revealed that TIME_ACT-high regions exhibit dense lymphocyte infiltration near tumor cells, indicating localized immune activation. Second, in 15 anti-PD1 transcriptomic cohorts spanning six cancer types, TIME_ACT outperforms 22 established signatures and methods, achieving a mean AUC of 0.76 and a clinically meaningful mean odds ratio of 6.11. Thirdly, TIME_ACT scores can be accurately inferred from tumor histopathology slides. Finally, slide-inferred TIME_ACT scores predict ICB response across eight unseen cohorts, achieving a mean AUC of 0.72 and a mean odds ratio of 5.02. These findings establish TIME_ACT as a robust, pan-cancer, and low-cost predictor of ICB response.

Introduction

Immune checkpoint blockade (ICB) therapies have transformed the landscape of cancer immunotherapy, yielding considerable clinical benefits in a subset of patients across multiple cancer types [1–5]. Among these, melanoma and non-small cell lung cancer (NSCLC) exemplify a prototypical immunogenic tumor where ICB has demonstrated remarkable therapeutic success [6,7]. Despite this progress, a substantial fraction of patients do not respond, underscoring an unmet need for predictive biomarkers that can guide treatment decisions and improve patient stratification [8]. Importantly, a critical unmet challenge is identifying which tumors possess sufficient immune activation to benefit from ICB therapy.

A key determinant of ICB efficacy is the tumor microenvironment (TME), which plays a central role in modulating anti-tumor immunity [9–11]. TME exhibits considerable heterogeneity and has been broadly categorized as “Hot” and “Cold” immunophenotypes [12]. Hot tumors are enriched with tumor-infiltrating lymphocytes (TILs), exhibit high expression of immune checkpoints, and demonstrate active inflammatory signaling, robust antigen presentation, and elevated cytotoxic T lymphocyte (CTL) activity, characteristics generally associated with better responses to ICB [7]. In contrast, cold tumors are immunologically inactive, characterized by sparse immune infiltration, impaired antigen processing, and low expression of interferon-stimulated genes and chemokines, contributing to immune evasion and therapy resistance [7]. While it is challenging to distinguish between the presence of immune cells and functional immune activity, several studies have attempted to classify hot and cold tumors [13–19]. Notably,

many of these studies have focused on one cancer type without studying their reproducibility across tumor types and cohorts, thus limiting their utility as broadly applicable predictive biomarkers. A critical unmet challenge, hence, is the development of a more general biomarker that identifies which individual tumors (independent of tumor type) possess sufficient immune activation to benefit from ICB therapy.

A variety of transcriptomic approaches based on immune-related signatures have been developed to predict ICB response, including IFN-γ-related signatures [20], T cell signatures [21,22], B cell signatures [23,24], and antigen presentation machinery–based scores [25,26]. Furthermore, several methods such as TIDE [27], IMPRES [28], SELECT [29], IPRES [30,31], IPS [32], COX_IS [33], etc., have been developed to capture tumor–immune dynamics or predict clinical response probabilities. However, these models often exhibit cohort-specific variable performance, and some rely on assumed mechanistic interpretations of response, without directly measuring the activation state of the TME [34,35]. While several immune-related transcriptomic signatures have been proposed, few have been specifically designed to comprehensively and robustly quantify tumor immune activation across diverse cancer types in a clinically generalizable manner.

To address these gaps, here we introduce TIME_ACT (Tumor Immune MicroEnvironment ACTivation), a robust and interpretable transcriptomic signature derived from TCGA melanoma samples using converging evidence of three previously established key measures of immune activation. Those include immune infiltration, inflammation, and TIL spatial patterns. Inferred in melanoma, where ICB treatments have been the most successful to date, TIME_ACT is designed to reflect functional immune engagement rather than the mere presence of immune cells. We first demonstrate that TIME_ACT generalizes to several cancer types beyond melanoma, enabling pan-cancer identification of immunologically hot tumors. Furthermore, we show that TIME_ACT robustly predicts anti-PD1 response in 15 different cohorts across 6 cancer types, outperforming 7 well-known previously published transcriptomic-based approaches, and 15 previously published immune-related signatures. We then leveraged Path2Omics [36–38], our recently developed deep learning model designed to predict transcriptomics from tumor H&E slides, to infer TIME_ACT scores directly from patients' histopathology slides. We show that the slide-inferred TIME_ACT score successfully predicts patient response to ICB therapies across 8 independent unseen datasets, close to the accuracy levels obtained from the scores based on actual measured tumor gene expression. These results underscore the clinical translational potential of TIME_ACT in advancing precision oncology in a timely and widely accessible manner using standard pathology slides, offering an exciting way to facilitate the matching of patients to ICB therapy going forward.

Results

Study design and datasets

We designed a multi-step computational framework to identify a transcriptomic signature of tumor immune activation. We then evaluated its predictive utility across both transcriptomic and histopathology data modalities. **(1)** Firstly, we stratified TCGA melanoma tumors into immune "Hot" and "Cold" groups based on consensus scoring across immune infiltration, inflammation, and TIL patch density, forming the basis for downstream gene signature derivation **(Fig. 1a)**. **(2)** In the second step, we identified genes upregulated in Hot tumors and enriched for immune-related pathways, resulting in a 66-gene expression signature termed *TIME_ACT*. This signature was then applied to additional TCGA tumor types to assess its pan-cancer relevance. Then, its ICB response prediction ability was evaluated in 16 independent transcriptomic cohorts of ICB-treated patients (15 anti-PD1 and 1 anti-CTLA4), spanning six different cancer types. Further, to characterize the biological basis of TIME_ACT, we performed co-expression network analysis, single-cell RNA-seq profiling, and spatial transcriptomics **(Fig. 1b)**. **(3)** In the third and final step, we extended this framework to histopathology using Path2Omics [36], an advanced deep learning approach that builds on our previously established DeepPT framework [38]. Path2Omics models can infer transcriptome-wide gene expression directly from H&E-stained whole-slide images. Applied to infer the gene expression in tumor slides from 8 new unpublished ICB patient's cohorts, TIME_ACT scores were subsequently computed from the slide-inferred transcriptomes to predict response **(Fig. 1c)**. Taken together, to our knowledge, this study represents the first computational framework predicting ICB response directly from pathology slides across multiple cancer types in an unsupervised approach. Notably, the latter mitigates the risk of over-fitting and is thus more likely to generalize more robustly to different cohorts.

(a) *Step 1: TCGA melanoma samples "Hot" and "Cold" immune phenotype classification*

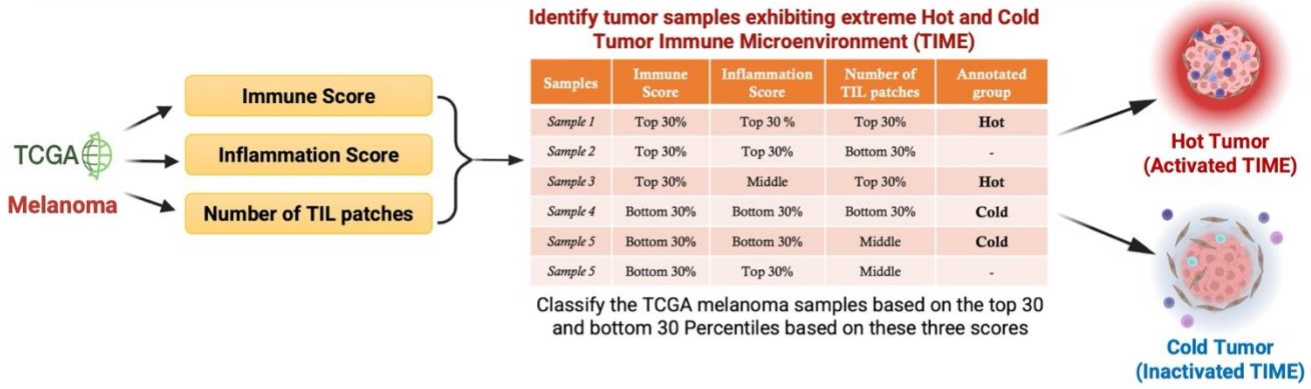

Samples	Immune Score	Inflammation Score	Number of TIL patches	Annotated group
Sample 1	Top 30%	Top 30 %	Top 30%	**Hot**
Sample 2	Top 30%	Top 30%	Bottom 30%	-
Sample 3	Top 30%	Middle	Top 30%	**Hot**
Sample 4	Bottom 30%	Bottom 30%	Bottom 30%	**Cold**
Sample 5	Bottom 30%	Bottom 30%	Middle	**Cold**
Sample 5	Bottom 30%	Top 30%	Middle	-

(b) *Step 2: Derivation of Tumor Immune Microenvironment Activation (TIME_ACT) Gene Signature and its application to predict ICB response from patient transcriptomics data*

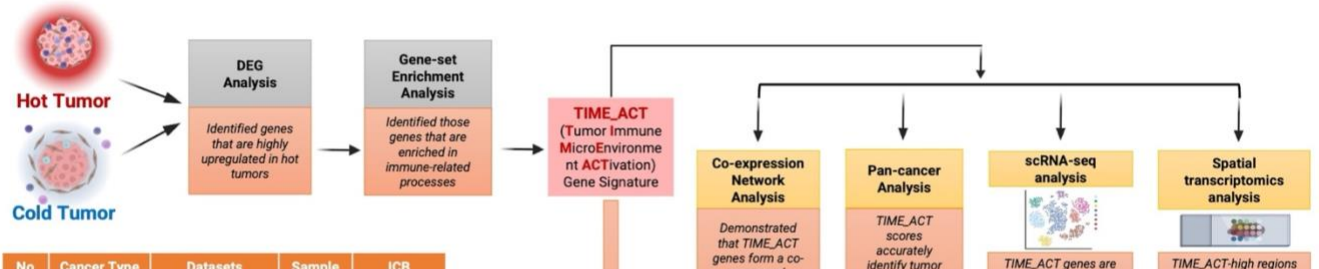

No	Cancer Type	Datasets	Sample Size	ICB Treatment
1	Breast cancer	phs002419	14	anti-PD1
2	Breast cancer	PRJNA558949	50	anti-PD1
3	ccRCC	EGAS00001004353	354	anti-PD1
4	ccRCC	phs001493	29	anti-PD1
5	HNSCC	GSE159067	102	anti-PD1
6	HNSCC	GSE195832	20	anti-PD1
7	HNSCC	phs001623	24	anti-PD1
8	Melanoma	GSE160638	28	anti-PD1
9	Melanoma	GSE91061	49	anti-PD1
10	Melanoma	PRJEB23709	41	anti-PD1
11	Melanoma	PUCH_cohort	55	anti-PD1
12	Melanoma	phs000452.v2.p1	42	anti-CTLA4
13	Mesothelioma	phs002207	16	anti-PD1
14	NSCLC	GSE126044	16	anti-PD1
15	NSCLC	GSE135222	27	anti-PD1
16	NSCLC	phs002822	118	anti-PD1

	Patient 1	Patient 2	...
Gene 1	10.33	5.38	...
Gene 2	11.07	6.38	...
...	...	...	...

	TIME_ACT score
Patient 1	0.46
Patient 2	-0.13
...	...

(c) *Step 3: Predicting expression of TIME_ACT genes and ICB treatment response directly from pathology slides*

Tumor pathology slide

Path2Omics

No.	Cohort name	Treatment	#Slides	Source
1	NCI-BLCA	ICB	48	NCI *(Unpublished)*
2	Cedars-Sinai SKCM	ICB	35	Cedars-Sinai *(Unpublished)*
3	Cedars-Sinai BRCA	ICB	23	Cedars-Sinai *(Unpublished)*
4	Cedars-Sinai LUAD	ICB	30	Cedars-Sinai *(Unpublished)*
5	HCRN-KIRC	ICB	151	HCRN *(Unpublished)*
6	HCRN-KIRP	ICB	48	HCRN *(Unpublished)*
7	Taiwan-HNSCC$_1$	ICB	33	NYCU Taiwan *(Unpublished)*
8	Taiwan-HNSCC$_2$	ICB	61	NYCU Taiwan *(Unpublished)*
	Total		**429**	

Slide-inferred Gene Expression

	Slide1	Slide2	Slide3
Gene 1	10.33	5.38	2.32
Gene 2	11.07	6.38	8.45
...	...	...	...

	TIME_ACT score
Slide 1	0.46
Slide 2	-0.13
...	...

Fig. 1 | Multi-modal analytical framework for developing and validating the TIME_ACT signature and predicting ICB response. (a) Schematic overview of immune phenotype classification in TCGA melanoma using three orthogonal immune features: Immune Score, Inflammatory Response Score, and Number of TIL patches. **(b)** TIME_ACT's ability to identify 'hot' vs 'cold' labeled tumors was identified across additional TCGA cancer types on which it was never trained. Its ability to predict ICB response was then evaluated in 16 independent transcriptomic cohorts of ICB-treated patients (15 anti-PD-1 and 1 anti-CTLA-4). To further investigate the biological basis of TIME_ACT, we performed co-expression network analysis, single-cell RNA-seq profiling, and spatial transcriptomics to uncover its cell-type specificity and spatial localization within the tumor microenvironment. **(c)** To extend TIME_ACT ICB prediction to histopathology, we applied Path2Omics, a deep learning framework trained on TCGA slides, to infer gene expression directly from H&E-stained images. TIME_ACT scores computed from the slide-inferred expression of TIME_ACT genes were then used to predict ICB response across 8 unpublished, unseen clinical cohorts, enabling the first-of-its-kind unsupervised cross-cancer prediction of ICB outcome directly from pathology images.

Identifying the TIME_ACT signature via an integrative analysis in the TCGA melanoma cohort

To identify tumor immune activation signatures, we first selected melanoma as our discovery cohort due to its well-characterized immunogenicity and relatively high response rate to ICB therapies [12,39]. Specifically, we leveraged three existing orthogonal metrics of immune activity in the TIME: (i) the Immune Score [40], representing the degree of immune infiltration; (ii) the Inflammation Score [41], indicating cytokine-mediated immune activation; and (iii) the number of TIL Patches [42], quantifying the number of spatially distinct immune-enriched regions in the tumor. Together, these three metrics capture overall levels and spatial dimensions of immune engagement. We found that 363 TCGA-SKCM (melanoma) samples had complete data for all three scores. Then, we used an aggregate ranking across all three metrics for each tumor in the TCGA melanoma cohort (see Methods for details) to assess overall immune activation. Tumors in the top 30% across these metrics were defined as *immune-active ("Hot")*, and those in the bottom 30% as *immune-inactive ("Cold")* **(Fig. 1a)**. This approach identified 66 Hot and 49 Cold tumors, yielding a total of 115 tumors, representing approximately 32% of the cohort size, providing an adequate sample size while maintaining stringent classification to enable robust downstream comparisons between tumors with clearly active or inactive immune landscapes. The middle 40% of the TCGA samples were excluded to avoid phenotype ambiguity and to ensure a stringent contrast between Hot and Cold groups.

Differential gene expression (DGE) analysis comparing Hot (n=66) and Cold (n=49) tumors identified 252 genes that were significantly highly upregulated in Hot tumors **(Extended Data Table 1)**, filtered using stringent thresholds (top 20% of upregulated genes in DGE analysis selected based on

both log_2FC and Bayesian B-value: $log_2FC > 3.66$ and $B > 48.5$) **(Fig. 2a)**. Furthermore, functional enrichment analysis revealed that these genes were significantly involved in immune-related biological processes such as T cell activation, lymphocyte differentiation, and cytokine signaling **(Extended Data Table 2)**. We further refined this gene list by selecting only those involved in the top 10 most significantly enriched immune-related processes (adjusted p-value < 0.05) **(Fig. 2b)**, as our goal was to identify genes crucial for activating the immune components of TME in Hot tumors. This filtering yielded a curated set of 66 genes, which we defined as the "*TIME_ACT signature"* **(Extended Data Table 3)**. Further, analyzing a single-cell RNA-seq (scRNA-seq) dataset (GSE115978) from melanoma patient samples [43] demonstrated that TIME_ACT genes are predominantly expressed in immune cell populations, particularly T cells, B cells, and dendritic cells, while showing minimal expression in malignant cells, fibroblasts, and cancer-associated fibroblasts (CAFs) **(Fig. 2c)**. This immune cell specificity reinforces the signature's relevance to the TIME.

To investigate whether these 66 genes represent a coherent biological program rather than a random collection of immune-associated genes, we performed a Weighted Gene Co-expression Network Analysis (WGCNA) on the top 10,000 most variable genes across TCGA melanoma samples. This analysis identified multiple gene modules **(Extended Data Fig. 1a)**, among which the turquoise module emerged as the most strongly associated with the Hot phenotype (module eigengene $p = 3.36e\text{-}40$) **(Extended Data Fig. 1b)**. Importantly, all 66 TIME_ACT genes clustered within this turquoise module, underscoring their functional relatedness. To further quantify their centrality, we computed module membership scores (kME), which measure the correlation of each gene with the module eigengene. TIME_ACT genes exhibited significantly higher kME scores than other genes in the same module ($p = 4.94e\text{-}71$) **(Extended Data Fig. 1c)**, indicating that they are not only co-expressed but also represent core "hub" genes within this immune-activated transcriptional network. These results confirm that TIME_ACT genes are functionally connected and topologically central within a network specifically enriched in Hot tumors, providing strong evidence that they define a biologically meaningful immune activation signature.

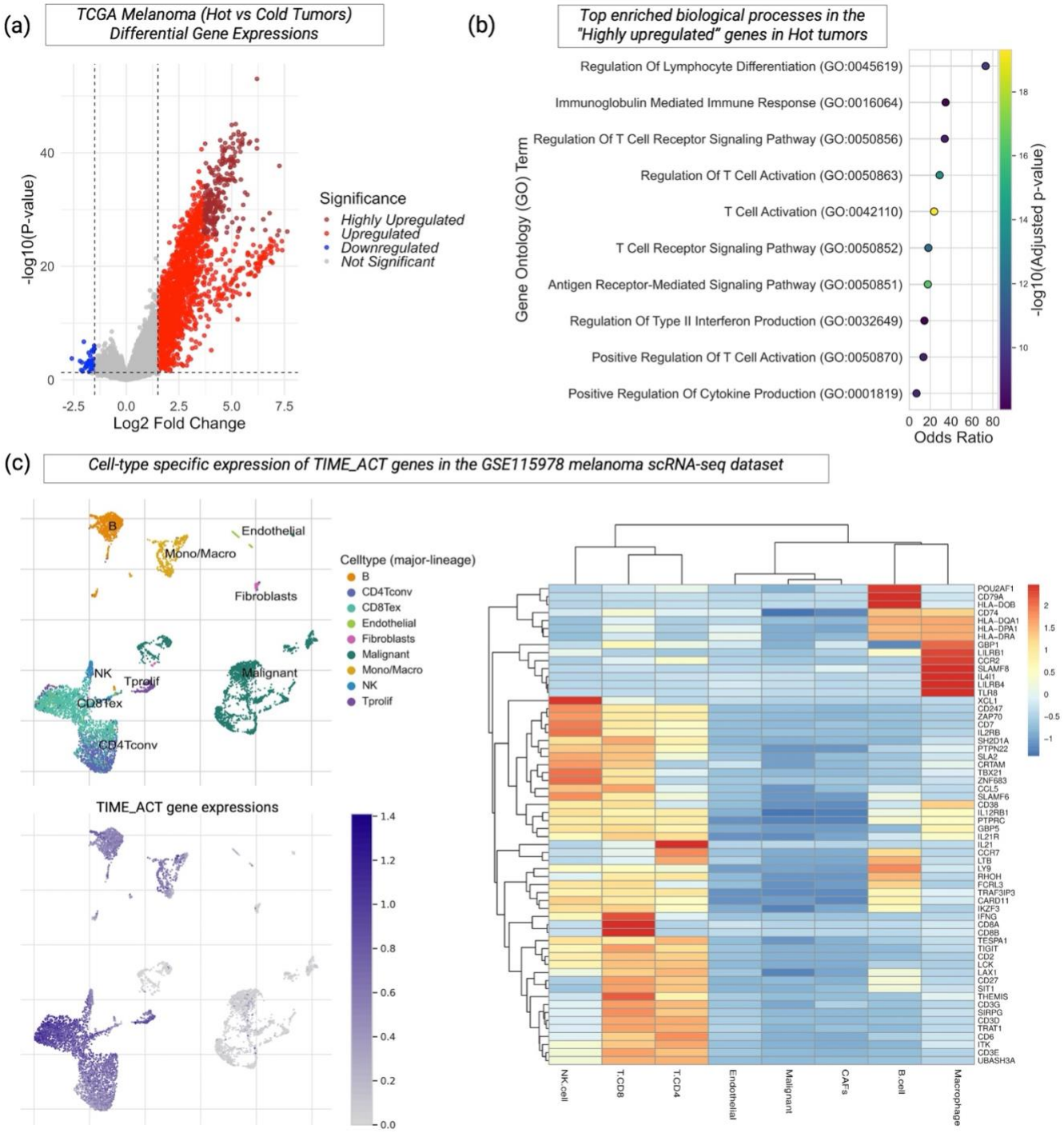

Fig. 2 | Derivation of the TIME_ACT signature by integrating immune phenotyping and transcriptomic data in melanoma. **(a)** Volcano plot showing differentially expressed genes between Hot and Cold tumors. A total of 252 genes that are upregulated in Hot vs Cold tumors were selected based on stringent thresholds for both $\log_2$FC (>3.66) and B-statistic (>48.5). **(b)** Gene ontology enrichment analysis of the 252 upregulated genes using Enrichr. The 66 TIME_ACT genes were selected

based on membership in the top ten immune-related GO Biological Process terms enriched in the 252 upregulated genes (FDR < 0.05). **(c)** Cell-type-specific expression of TIME_ACT genes in the GSE115978 single-cell RNA-seq melanoma dataset was retrieved from the TISCH2 database. The left upper panel shows UMAP clustering of transcriptionally defined cell populations. The left bottom panel overlays the same UMAP with TIME_ACT gene expression, where the intensity of purple indicates higher aggregate expression of TIME_ACT genes. The right panel represents the expression heatmap of the 66 TIME_ACT genes (y-axis) across this dataset, with the x-axis displaying different cell types. As evident, the latter are predominantly expressed in immune cell populations, including T cells and B cells, and are minimally expressed in malignant cells and fibroblasts, supporting their immune-specific role within the TME.

TIME_ACT scores accurately identify tumor immune activation in other cancer types

To investigate the potential applicability of the 66-gene TIME_ACT signature in other cancer types, we studied its ability to accurately classify Hot versus Cold tumors in each cancer type. We focused on eight TCGA cancer types, where corresponding immune, inflammation, and TIL patch scores were available, enabling us to form ground truth 'hot' and 'cold' labels in these cancer types (**Extended Data Table 4**). Accordingly, using the same top and bottom 30% strategy applied to these three scores in melanoma, tumors in each of these cancer types were annotated as Hot or Cold based on composite immune profiling, to generate a 'ground truth' dataset of annotated Hot and Cold tumors. Given these ground truth labels, we then tested the ability of the melanoma-derived TIME_ACT signature to distinguish these annotated groups. We implemented a single-sample gene set enrichment analysis (ssGSEA) using the 66-gene TIME_ACT signature to derive a TIME_ACT score for each sample (see Methods).

Higher TIME_ACT scores indicate stronger immune activation and are characteristic of immune-hot tumors **(Fig. 3a)**. Remarkably, the TIME_ACT scores demonstrated very high classification accuracy in all cancer types, ranging from 0.96 (for STAD) to 1.00 (BRCA and CESC) AUC **(Fig. 3b, left)**, showing that the melanoma-derived signature accurately captures immune activation in diverse TMEs. To further test the robustness of the signature, we applied it to two independent datasets[44] (GSE161537-NSCLC and GSE159067-HNSCC), where gene expression data were available, and each tumor sample had been pre-annotated as Hot or Cold. Reassuringly, also in both these external cohorts, the TIME_ACT score showed excellent prediction accuracy, achieving AUC values of 0.98 (for GSE161537-NSCLC) and 0.96 (for GSE159067-HNSCC) (**Fig. 3b, right)**. These results suggest that the melanoma-derived TIME_ACT signature is not only robust across cancer types but also transferable across cohorts, platforms, and study designs.

Next, to evaluate the fraction of Hot tumors in numerous other cancer types, we computed the TIME_ACT scores for all TCGA samples **(Extended Data Table 5).** To enable consistent cross-cancer

comparisons, we established a single pan-cancer cut-off by pooling data from nine tumor types, including melanoma and eight additional cancers, where we annotated the Hot and Cold labels. Using the Youden Index, we identified an optimal threshold of 0.0655 that maximally separates Hot and Cold tumors based on TIME_ACT scores **(Fig. 3c)**. Notably, in all analyses shown in the following in this paper, this threshold was kept fixed and applied uniformly across the TCGA and any other patients' datasets analyzed herewith.

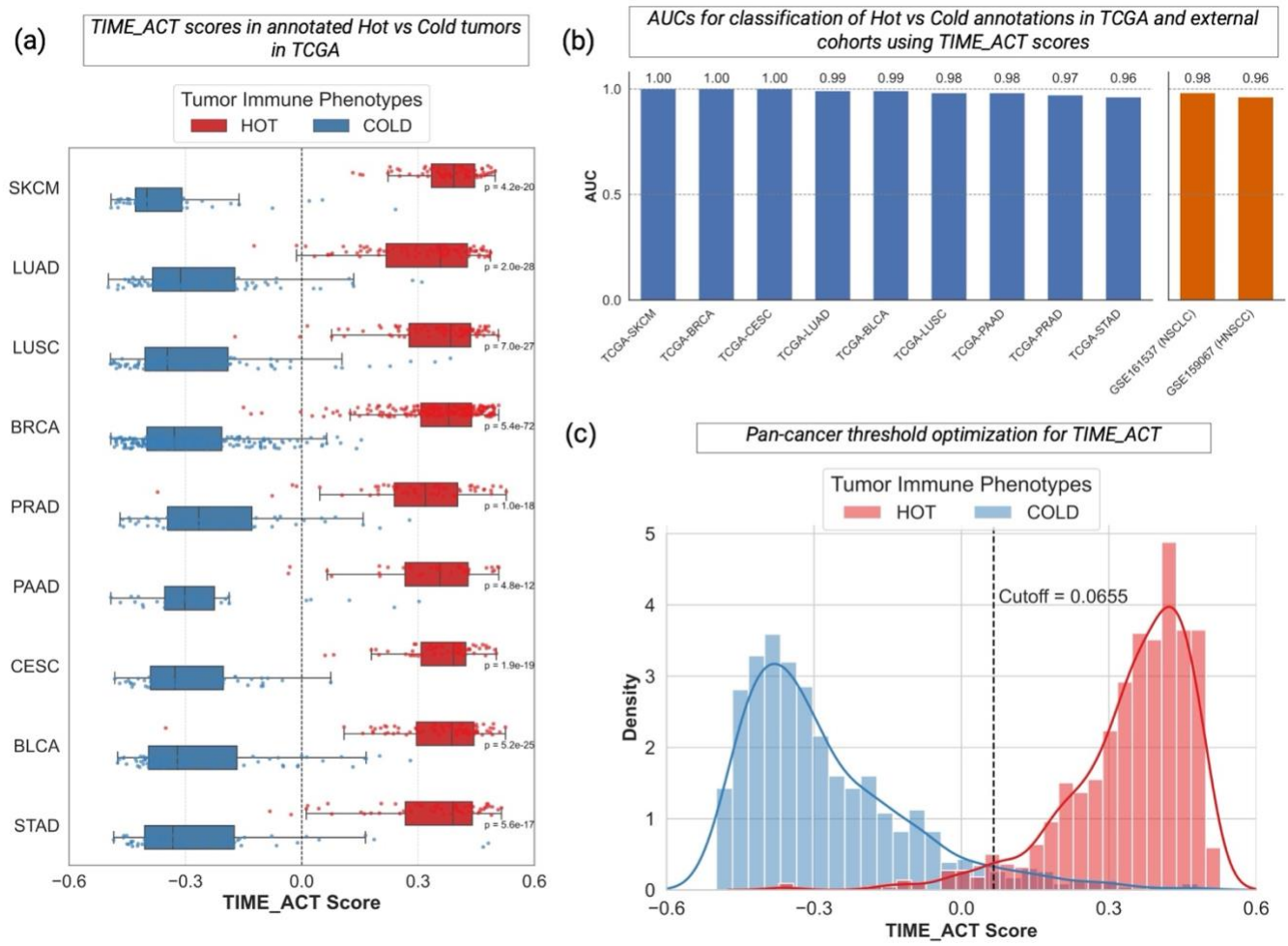

Fig. 3 | TIME_ACT defines a robust transcriptomic biomarker of tumor immune activation across cancer types. **(a)** Distribution of TIME_ACT scores in Hot and Cold annotated tumors across nine TCGA cancer types with annotated ground truth, showing consistently markedly higher scores in the originally annotated hot tumors. **(b)** Bar plot summarizing AUC of classifying Hot vs. Cold annotated tumors across the nine annotated TCGA cancer types using the TIME_ACT signature (in blue) and in two independent datasets with ground truth annotated Hot/Cold labels, GSE161537 (NSCLC) and GSE159067 (HNSCC) (in orange). All cohorts demonstrated strong discriminatory accuracy (AUCs ≥ 0.96). **(c)** Pan-cancer

optimization of the TIME_ACT classification threshold using Youden's index across pooled Hot and Cold samples from nine TCGA cancer types.

Studying the biological bases of the TIME_ACT signature at bulk, single-cell, and spatial resolutions

To further contextualize the biological basis of TIME_ACT and assess its cross-tumor applicability, we performed an integrative, pan-cancer analysis leveraging bulk transcriptomics, immune subtyping, single-cell datasets, and spatial data across diverse cancer types. First, we obtained the immune subtype annotations and cell-type abundance estimates from the TCGA immune landscape resource described by Thorsson et al. [45], which used pan-immune gene expression features and deconvolution-based immune cell estimates and classified tumors into 6 different immune subtypes (C1–C6). To test whether TIME_ACT scores tracked with these established immune-active phenotypes, we examined the distribution of immune subtypes in TIME_ACT-defined Hot tumors. The majority of Hot tumors fell into immune-active subtypes, either the C2 (IFN-γ dominant; 40.1%) or C3 (inflammatory; 30.2%) **(Fig. 4a)**, both of which are associated with elevated cytotoxicity, antigen presentation, and lymphocyte infiltration. Consistent with this, TIME_ACT scores showed strong correlations with key pan-cancer immune signatures, including IFN-γ response, lymphocyte infiltration, TCR and BCR richness, and leukocyte fraction **(Fig. 4b)**. Together, these findings further signify that the TIME_ACT signature reliably captures tumors with immune-inflamed phenotypes characterized by active antitumor immune responses across cancer types.

We then tested whether TIME_ACT genes consistently localize to immune compartments at the single-cell level across tumor types, extending our previous analysis in melanoma. Consistently, we find that TIME_ACT genes remained preferentially expressed in immune cells, particularly T cells, B cells, and dendritic cells, and were rarely expressed in malignant or stromal compartments **(Extended Data Fig. 2)**. Given this strong immune-cell specificity, we next asked whether TIME_ACT scores correlate with the abundance of immune cell types known to mediate antitumor immunity, using deconvolved bulk transcriptomic data from TCGA. Across cancer types, TIME_ACT was positively correlated with $CD8^+$ T cells, M1 macrophages, and Th1 cells, immune subsets canonically associated with pro-inflammatory and cytotoxic activity **(Fig. 4c)**. In contrast, TIME_ACT scores were negatively correlated with resting or undifferentiated populations, including M0 macrophages, resting NK cells, and resting mast cells. These associations indicate that TIME_ACT preferentially reflects active immune engagement rather than overall immune cell presence.

Finally, we aimed to identify the key spatial relations between different cell-types in the TME that are associated with immune activation (as quantified by TIME_ACT scores). To this end, we analyzed breast cancer tissue sections, both formalin-fixed paraffin-embedded and fresh-frozen, from the 10x Genomics public spatial transcriptomics repository. Each spatial spot in this cohort was previously annotated by expert pathologists to classify tumor cells, stromal cells, lymphocytes, and macrophages. TIME_ACT scores were computed per spot, and those exceeding the pan-cancer threshold (≥ 0.0655) were designated as hot. In both samples, we observed that high TIME_ACT-scoring regions tended to co-localize with spots enriched in dense lymphocyte aggregations that are adjacent to malignant areas **(Fig. 4d)**. This analysis testifies to a spatial coherence between transcriptomically inferred immune activation and histologically defined lymphocyte localization in the TME.

Next, to quantify spatial immune engagement at high resolution, we analyzed the TCGA-BRCA cohort using the panopTILs resource [46,47], which provides pathologist-annotated lymphocyte, tumor, and stromal cell regions for a large cohort of 151 patients' whole-slide images. We calculated nearest-neighbor distances (NNDs) between each lymphocyte and the closest cancer or stromal cell, focusing on contacts within a focused region of a 150 pixels radius. TCGA-BRCA samples were stratified based on TIME_ACT scores, and the top 20% (Hot) and bottom 20% (Cold) tumors were compared. Hot tumors exhibit significantly shorter cancer–lymphocyte distances than cold tumors ($p = 2.44e-02$), reflecting enhanced immune–tumor contact **(Fig. 4e)**. Stromal–lymphocyte distances showed a similar but weaker trend ($p = 4.84e-02$). We then quantified the fraction of cancer cells with nearby lymphocytes and correlated this score with TIME_ACT expression. Tumors with a higher frequency of cancer–lymphocyte spatial proximity showed significantly elevated TIME_ACT scores (Spearman $\rho = 0.50$, $p = 1.01e-03$), further testifying that TIME_ACT captures the degree of local tumor-immune engagement. Stromal–lymphocyte proximity was only modestly correlated ($\rho = 0.22$, $p = 1.3e-02$), while cancer–stroma contacts, used as a negative control, were indeed negatively associated with TIME_ACT ($\rho = -0.15$, $p = 4.8e-01$) **(Fig. 4f)**. Together, these findings demonstrate that TIME_ACT reflects not only molecular programs of immune activation but also can be applied to uncover meaningful spatial relationships between immune and malignant cells, reinforcing its role as a multiscale biomarker of inflamed TMEs.

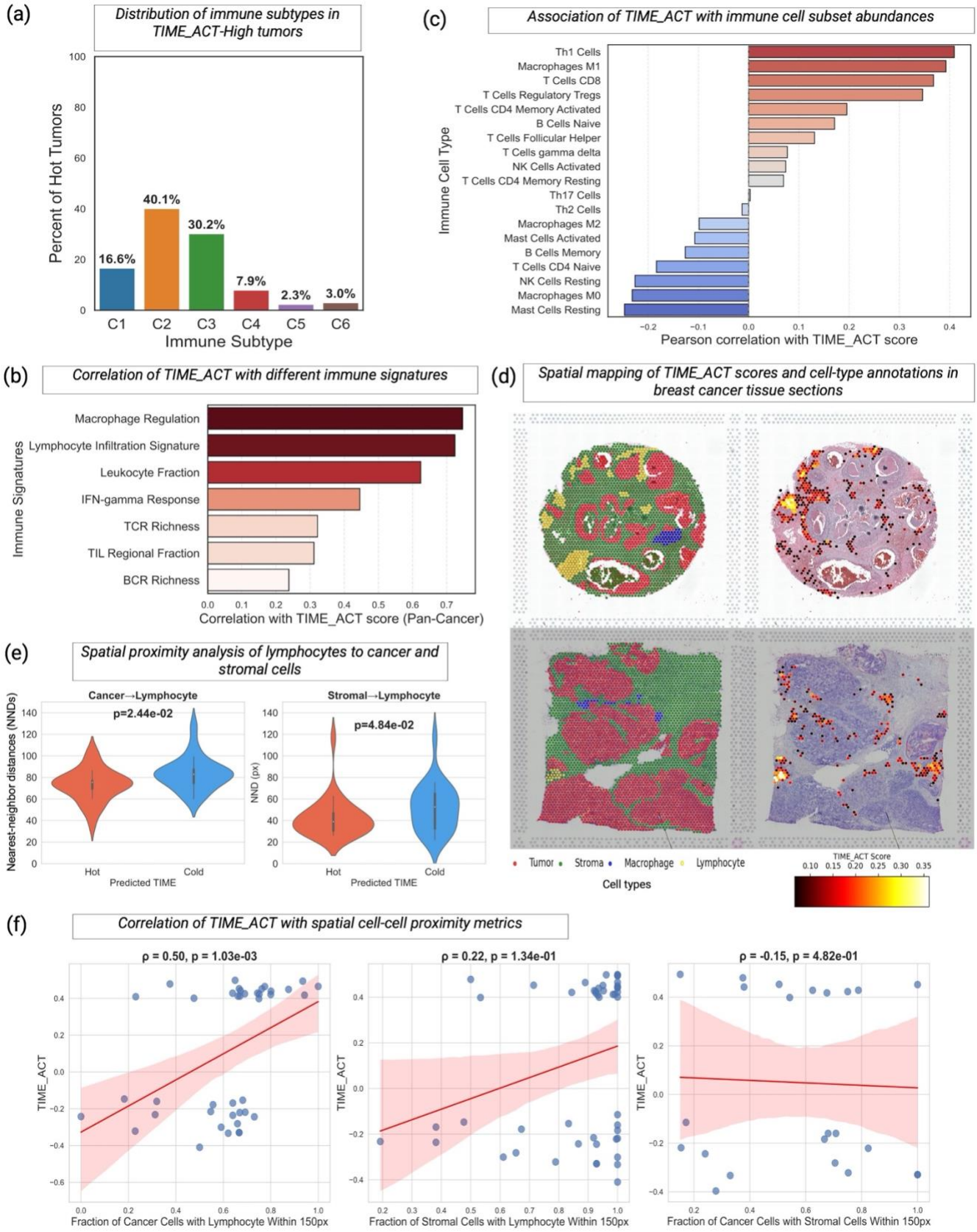
(a)
Distribution of immune subtypes in TIME_ACT-High tumors
Percent of Hot Tumors
16.6%
40.1%
30.2%
7.9%
2.3%
3.0%
C1
C2
C3
C4
C5
C6
Immune Subtype
(c)
Association of TIME_ACT with immune cell subset abundances
Immune Cell Type
Th1 Cells
Macrophages M1
T Cells CD8
T Cells Regulatory Tregs
T Cells CD4 Memory Activated
B Cells Naive
T Cells Follicular Helper
T Cells gamma delta
NK Cells Activated
T Cells CD4 Memory Resting
Th17 Cells
Th2 Cells
Macrophages M2
Mast Cells Activated
B Cells Memory
T Cells CD4 Naive
NK Cells Resting
Macrophages M0
Mast Cells Resting
Pearson correlation with TIME_ACT score
(b)
Correlation of TIME_ACT with different immune signatures
Immune Signatures
Macrophage Regulation
Lymphocyte Infiltration Signature
Leukocyte Fraction
IFN-gamma Response
TCR Richness
TIL Regional Fraction
BCR Richness
Correlation with TIME_ACT score (Pan-Cancer)
(d)
Spatial mapping of TIME_ACT scores and cell-type annotations in breast cancer tissue sections
Tumor
Stroma
Macrophage
Lymphocyte
Cell types
TIME_ACT Score
(e)
Spatial proximity analysis of lymphocytes to cancer and stromal cells
Cancer→Lymphocyte
p=2.44e-02
Nearest-neighbor distances (NNDs)
Hot
Cold
Predicted TIME
Stromal→Lymphocyte
p=4.84e-02
NND (px)
Hot
Cold
Predicted TIME
(f)
Correlation of TIME_ACT with spatial cell-cell proximity metrics
ρ = 0.50, p = 1.03e-03
TIME_ACT
Fraction of Cancer Cells with Lymphocyte Within 150px
ρ = 0.22, p = 1.34e-01
TIME_ACT
Fraction of Stromal Cells with Lymphocyte Within 150px
ρ = -0.15, p = 4.82e-01
TIME_ACT
Fraction of Cancer Cells with Stromal Cells Within 150px

Fig. 4 | Multiscale characterization of TIME_ACT across immune subtypes, cellular composition, and spatial localization in diverse cancer types. **(a)** Distribution of immune subtypes among TIME_ACT-defined Hot tumors across the TCGA pan-cancer cohort. Hot tumors are predominantly classified as C2 (IFN-γ dominant) and C3 (inflammatory) subtypes, known for immune-inflamed phenotypes. **(b)** Correlation of TIME_ACT scores with established immune-related signatures across cancers, including IFN-γ response, lymphocyte infiltration, TCR/BCR richness, and leukocyte fraction, demonstrating alignment with active immune microenvironments. **(c)** Association of TIME_ACT scores with immune cell subset abundance from deconvolved TCGA data. Positive correlations were observed with $CD8^+$ T cells, M1 macrophages, and Th1 cells; negative correlations with resting immune populations such as M0 macrophages and resting NK cells. **(d)** Spatial transcriptomics analysis of breast cancer tissue sections from the 10x Genomics repository shows that TIME_ACT-high (hot) regions are enriched in lymphocyte-dense areas adjacent to tumor epithelium. **(e)** Pathology-based spatial proximity analysis of TCGA-BRCA H&E slides using panopTILs reveals significantly reduced cancer–lymphocyte distances in TIME_ACT-hot tumors compared to cold tumors, suggesting enhanced immune infiltration. **(f)** TIME_ACT scores positively correlate with cancer–lymphocyte proximity, modestly with stromal–lymphocyte proximity, and show no significant association with cancer–stroma proximity, confirming the immune-focused spatial relevance of the signature.

TIME_ACT outperforms extant transcriptomic-based biomarkers of ICB response prediction

To assess whether TIME_ACT scores in tumors with confirmed immune activation associate with clinical benefit from ICB, we first examined the objective response rates (ORRs) to anti-PD-1/PD-L1 therapy across nine cancer types. Specifically, we focused on the TIME_ACT scores of tumor samples that were annotated as “Hot” based on three orthogonal immune phenotyping metrics applied in earlier steps. We then studied whether higher mean TIME_ACT scores among these Hot tumors correlate with higher ORRs across cancer types. ORR data were retrieved from our previous studies [48,49]. Among the nine cancer types evaluated, eight had both ORR and TIME_ACT data available. Remarkably, we observed a strong positive correlation between the mean TIME_ACT score of Hot tumors and the corresponding ORR (Pearson r = 0.72, $p = 4.46e\text{-}02$; **Fig. 5a**), suggesting that tumors with more pronounced immune activation, as captured by TIME_ACT, are more likely to respond to ICB therapy. These findings underscore the translational potential of the TIME_ACT signature as a pan-cancer biomarker of immune activation and ICB response, setting the stage for the next steps of our further analysis.

We next assessed the value of TIME_ACT scores in predicting patient response to ICB based on pre-treatment transcriptomic data from 15 independent anti-PD-1 cohorts [50–64] **(Extended Data Table 6)**. Starting with melanoma, we find that TIME_ACT scores robustly stratify responders from non-responders

in the four publicly available pre-treatment anti-PD1 cohorts, with a mean AUC of 0.77, ranging from 0.66 to 0.84. In the two melanoma anti-PD1 cohorts with both pre-treatment and on-treatment samples (GSE91061 and PRJEB23709) [50,51], TIME_ACT scores achieved AUCs of 0.66 (for GSE91061) and 0.84 (for PRJEB2370) based on the pre-treatment transcriptomics data. However, its performance improved markedly in the corresponding on-treatment samples, reaching 0.75 (for GSE91061) and 0.93 (for PRJEB23709) **(Extended Data Fig. 3a)**. These results demonstrate that TIME_ACT not only reflects pre-existing immune activity but also sensitively captures early immunologic changes induced by anti-PD1 therapy. Further, in an anti-CTLA-4-treated melanoma cohort (phs000452) [65], TIME_ACT also performed well, yielding an AUC of 0.72. These findings validate the signature's predictive value in both PD-1 and CTLA-4-based therapies in melanoma. We then extended our analysis to evaluate the predictive power of TIME_ACT in five additional cancer types beyond melanoma **(Extended Data Fig. 3b)**. TIME_ACT consistently predicted anti-PD1 response across all 15 pre-treatment cohorts, achieving a mean AUC of 0.76. Among individual cancer types, the mean AUC was 0.79 in NSCLC (3 cohorts), 0.78 in HNSCC (3 cohorts), and 0.76 in breast cancer (2 cohorts) **(Fig. 5b, left)**. Notably, all these cohorts were not used in identifying the TIME-ACT signature and hence reliably serve as independent test cohorts that measure its generalizability and real-world performance accuracy.

Across the 15 independent pre-treatment anti-PD-1 cohorts, responders consistently exhibited significantly higher TIME_ACT scores than non-responders (**Extended Data Fig. 3c**), highlighting the signature's strong association with clinical benefit. To further quantify this association in a clinically interpretable way, we used odds ratios (ORs), which measure the strength of enrichment of responders among biomarker-defined groups. Specifically, the OR compares the fraction of true responders in the group of patients predicted to be 'responders' with that in the predicted 'non-responder' group. To this end, we applied the previously defined pan-cancer threshold (0.0655) as is to stratify patients in each ICB clinical cohort we studied into TIME_ACT-High (Hot) and TIME_ACT-Low (Cold) groups. We applied this threshold to stratify tumors in of the 15 independent pre-treatment anti-PD-1 datasets described above into these two groups and calculated the corresponding ORs for treatment response. The TIME_ACT-based classification yielded strong odds ratios across multiple cancer types, mean odds ratios (OR) of 6.11, including 6.9 in melanoma, 7.85 in HNSCC, 4.24 in NSCLC, and 8.46 in breast cancer (**Fig. 5b, right**), indicating a significant enrichment of responders among TIME_ACT-High tumors. These findings emphasize the translational potential of TIME_ACT not only as a continuous signature but also as a threshold-based, clinically actionable predictor of response to PD-1/PD-L1 blockade across diverse tumor types.

Next, we compared TIME_ACT to a broad panel of 15 previously published immune-related gene signatures [21,23–26,66–72] that have been shown to predict ICB response, including IFNγ-responsive genes, immune cytolytic activity, T and B cell signatures, macrophages, antigen presentation machinery, and

pathways associated with TGFβ signaling **(Extended Data Table 7)**. TIME_ACT is the top-performing signature, with the highest mean AUC **(Fig. 5c)** and, importantly, the lowest coefficient of variation in predictive performance across all cohorts **(Extended Data Fig. 4a)**. We also compared TIME_ACT to 7 established transcriptomic-based predictors of ICB response [27–33,41], including TIDE [27], IMPRES [28], and SELECT [29]. Similarly, TIME_ACT consistently outperformed all 7 comparators in terms of both predictive accuracy and robustness, achieving the highest mean AUC **(Fig. 5d)** and the lowest variability across these datasets **(Extended Data Fig. 4b)**. Next, we performed a parallel comparison using the area under the precision–recall curve (AUPRC), a metric more sensitive to class imbalance in response data. The average AUPRC for TIME_ACT across the 15 pre-treatment anti-PD-1 cohorts was 0.63, higher than any other signature or method, indicating its superior ability to correctly prioritize true responders over non-responders in these largely imbalanced datasets **(Extended Data Fig. 4c-d)**. Together, these findings establish TIME_ACT as a reproducible, high-performing, and biologically informed transcriptomic biomarker that generalizes across cancer types and therapeutic contexts for the prediction of ICB response.

Given the widespread clinical use of tumor mutational burden (TMB) as a biomarker for immunotherapy response, we sought to additionally benchmark TIME_ACT against TMB in a subset of patients. However, among all 15 anti-PD-1 cohorts, only the Riaz et al. study [51] included both transcriptomic data and the necessary information for TMB calculation. Using this data, we found that TIME_ACT outperformed TMB in predicting ICB response, achieving an AUC of 0.66 versus 0.57 **(Extended Data Fig. 4e)**. Notably, TIME_ACT maintained predictive accuracy across both TMB-High (AUC = 0.64) and TMB-Low (AUC = 0.68) subgroups, underscoring its potential utility in TMB-low tumors where genomic biomarkers often underperform **(Extended Data Fig. 4f)**.

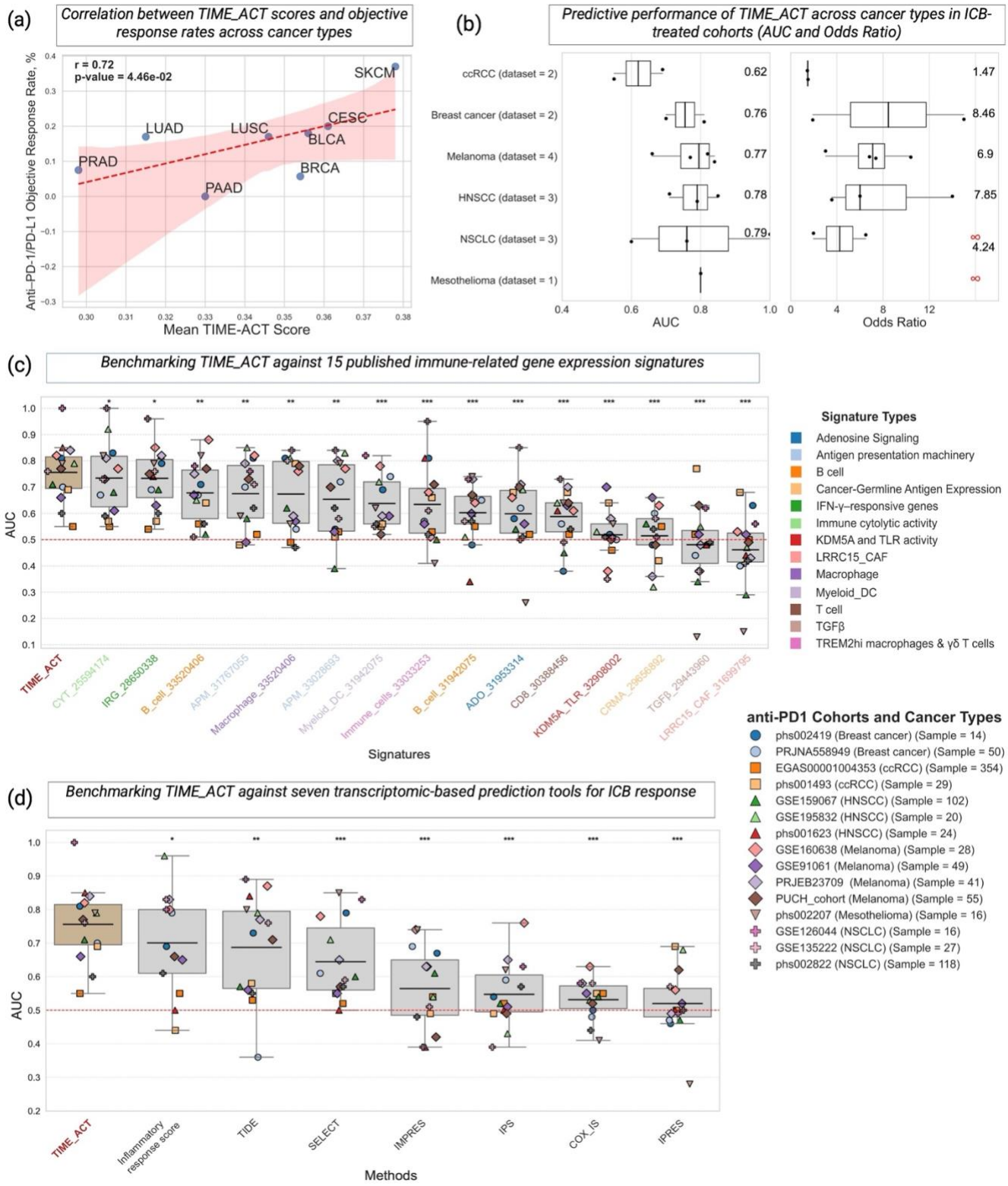

Fig. 5 | TIME_ACT performance in predicting patient response to anti-PD1 therapies from tumor gene expression. (a) Correlation between mean TIME_ACT scores in Hot tumors and objective

response rates (ORRs) to anti-PD-1/PD-L1 therapy across eight cancer types with available data. Higher immune activation, as captured by TIME_ACT, is associated with higher ORR. **(b)** Predictive performance of TIME_ACT across 15 independent anti-PD-1 pre-treatment transcriptomic cohorts, benchmarked using area under the ROC curve (AUC, left) and odds ratios (ORs, right) for response. TIME_ACT achieved high accuracy and enrichment of responders in TIME_ACT-High tumors across melanoma, NSCLC, HNSCC, and breast cancer. **(c)** Benchmarking TIME_ACT against 15 published gene signatures. The different signatures on the x-axis are represented by different colors, and the corresponding number for each signature indicates its PubMed ID. TIME_ACT achieved the highest mean AUC and lowest inter-cohort variability. Statistical significance for the comparison of TIME_ACT with each signature was calculated using a one-sided Wilcoxon signed-rank test ($p < 0.05$ = *, $p < 0.01$ = **, $p < 0.001$ = ***). **(d)** Comparison of TIME_ACT against 7 previously published transcriptomic-based prediction tools across all cohorts, showing the superior performance of TIME_ACT.

Predicting TIME_ACT scores and treatment response directly from histopathology

Tumor histopathology remains the most accessible and widely used diagnostic modality in oncology. Building on the superior performance of TIME_ACT in predicting treatment response from transcriptomic data, we explored the feasibility of inferring the expression of the 66 genes composing TIME_ACT and, based on that, computing TIME_ACT scores directly from pathology slides. Having these inferred scores, we then aimed to predict treatment response (**Fig. 1c**).

To this end, we first employed our recently developed Path2Omics framework [36], a deep learning model that extends the capabilities of the previously established DeepPT approach [38], to infer gene expression from pathology slides across 24 TCGA cancer types. To assess the inference accuracy, we calculated the Pearson correlation between inferred and actual expression levels for each of the TIME_ACT genes across all TCGA samples within each cancer type. Path2Omics demonstrated strong performance for the 66 TIME_ACT genes, with a median correlation of 0.61 on average across 24 cancer types, ranging from 0.45 (for PCPG) to 0.72 (for THCA) (**Fig. 6a**, **orange**). Notably, this performance was remarkably higher than that observed for all genes (**Fig. 6a, gray**), testifying that the TIME_ACT genes are among the most accurately inferred via Path2Omics.

We then computed TIME_ACT scores based on the slide-inferred gene expression and evaluated their ability to classify tumors into “Hot” and “Cold” categories, analyzing the TCGA cancer types with the ground truth Hot/Cold annotations. Remarkably, the slide-inferred TIME_ACT scores achieved AUC values exceeding 0.94 in all tested cancer types, closely matching the performance of TIME_ACT scores computed from actual measured expression data **(Fig. 6b)**. Taken together, these findings demonstrate that TIME_ACT gene expression and composite scores can be reliably inferred from pathology slides to a level that is sufficient for detecting tumor immune activation directly from the tumor pathology slides.

We next inferred the TIME_ACT scores of each patient directly from their tumor histopathology slides in a collection of 8 ICB clinical cohorts for which we had the slides and response data. Those include eight unpublished cohorts of patients treated with ICB, from multiple different medical centers, including datasets from our in-house NCI, Cedars-Sinai, HCRN (Hoosier Cancer Research Network) consortium, and NYCU-Taiwan. Notably, treatment response prediction based on the slide-inferred TIME_ACT scores achieved a mean AUC of 0.72, ranging from 0.65 (NCI BLCA cohort) to 0.8 (HCRN KIRP cohort) (**Fig. 6c, left panel**). The mean OR across these ICB datasets was 5.02, ranging from 1.78 (NCI BLCA cohort) to 12.75 (Taiwan HNSCC cohort) (**Fig. 6c, right panel**). **Extended Data Fig. 5a** shows the ROC curves for each individual cohort, and **Extended Data Fig. 5b** presents the distribution of slide-inferred TIME_ACT scores between responders and non-responders across cohorts.

Among all the slide-based cohorts we analyzed, matched RNA-seq data were available for the HCRN-KIRC cohort (dbGaP accession: phs003618.v1.p1). This enabled us to perform a direct comparison of the predictive performance of TIME_ACT scores derived from slide-inferred expression versus those computed from measured RNA-seq data. Remarkably, the slide-inferred TIME_ACT scores, based on histology-derived expression, matched the performance of RNA-seq-based scores (**Fig. 6d**). In the subset of matched HCRN-KIRC cohort (n = 82), TIME_ACT scores based on slide-inferred expression achieved an AUC of 0.76 and OR of 5.96, outperforming the scores derived based on RNA-seq-based expression data (AUC of 0.72 and OR of 4.52). One possible explanation for these quite surprising results may be that slide-based inference is less affected by technical variability and batch effects than RNA-seq data generated across multiple processing conditions. Taken together, these results underscore the robust predictive capability of the combined TIME_ACT and Path2Omics in predicting patient response directly from tumor pathology slides, offering a rapid and cost-effective alternative to traditional precision oncology omics-based tools.

Finally, we analyzed a cohort of 191 LUAD patients from Sheba Medical Center treated with ICB. Treatment response information was not available in terms of RECIST criteria, but only overall survival data were provided. We first stratified the patients into TIME_ACT-High (“Hot”) and TIME_ACT-Low (“Cold”) groups using the predefined pan-cancer threshold of 0.0655. We then performed a Kaplan-Meier survival analysis, which has demonstrated that patients with Hot tumors had significantly improved survival compared to those with Cold tumors (hazard ratio = 0.64, p = 2.5e-02; **Fig. 6e**), reflecting a 36% reduction in the risk of death. Taken together, these results testify to the translational promise of TIME_ACT as a functional immune activity score and its potential to stratify cancer patients to ICB treatment based on the immunological phenotype of their tumors.

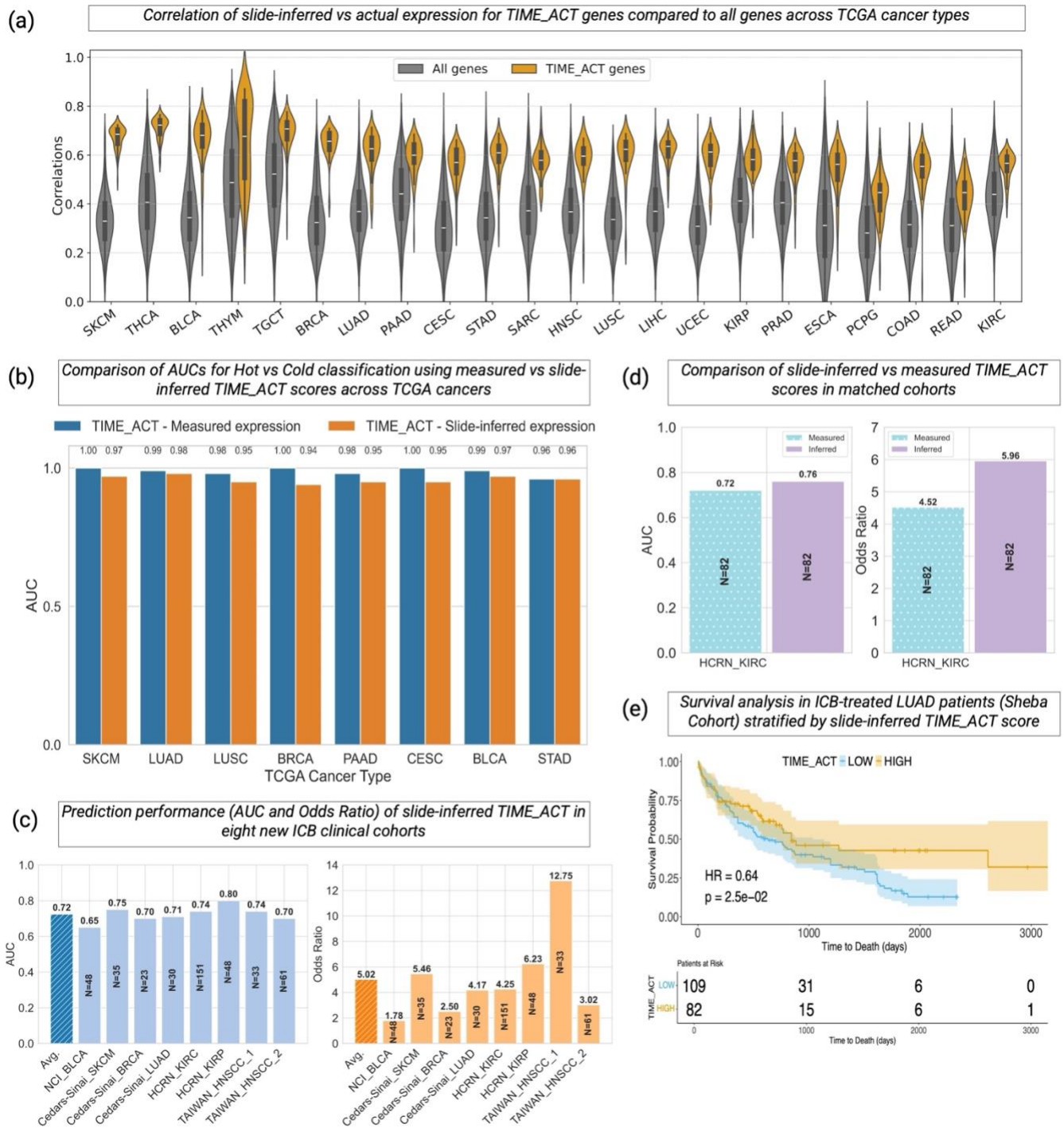

Fig. 6 | Predicting expression of TIME_ACT genes and treatment response directly from pathology slides. **(a)** Violin plots demonstrate the distribution of Pearson correlation coefficients between slide-inferred and measured RNA-seq expression for TIME_ACT genes (orange) versus all genes (gray) in different TCGA cancer types. **(b)** Bar plots show performance in predicting Hot vs. Cold tumors in different cancer types, based on slide-inferred TIME_ACT scores (orange) and TIME_ACT measured expression

(blue). AUC values for slide-inferred scores closely match those from RNA-seq-based scores. **(c)** Predictive performance of slide-inferred TIME_ACT scores in 8 independent ICB-treated clinical cohorts. AUC (left panel) and odds ratios (right panel) are shown across datasets. **(d)** Comparison of model performance using slide-inferred TIME_ACT scores versus those computed from the measured RNA-seq data in a subset of the HCRN-KIRC cohort. **(e)** Kaplan–Meier survival analysis of LUAD patients (n = 191, Sheba Medical Center cohort) stratified by slide-inferred TIME_ACT score using the pan-cancer threshold (0.0655). TIME_ACT-High (Hot) tumors were associated with significantly improved overall survival (hazard ratio = 0.64, p = 2.5e-02).

Discussion

Accurately predicting a patient's response to ICB remains an urgent unmet clinical need, as it is crucial for guiding optimal treatment decisions [1]. However, the existing transcriptomic biomarkers for ICB response often suffer from unstable performance on unseen datasets, limiting their clinical applicability [34,73,74]. This study presents TIME_ACT, a transcriptomic signature of tumor immune activation, which offers a simple, unsupervised approach for identifying immune-hot tumors and predicting therapeutic response to ICB treatments in many different cancer indications. Notably, the robust predictive power of TIME_ACT extends to digital pathology, maintaining a strong predictive power across diverse clinical settings. Using spatial transcriptomics and digital histopathology, we show that TIME_ACT-high regions co-localize with immune effector cells in direct proximity to tumor cells, reinforcing that the signature captures key spatial features of an inflamed TME.

Our study represents a comprehensive head-to-head benchmarking of a transcriptomic biomarker for pan-cancer ICB response prediction in multiple cohorts. Importantly, TIME_ACT not only achieved the highest mean AUC but also displayed the lowest inter-cohort variability, reinforcing its pan-cancer applicability and translational relevance. This performance extended to new clinical trial cohorts where TIME_ACT scores were inferred directly from histopathology slides, achieving predictive accuracy comparable to RNA-seq-derived scores. Thus, TIME_ACT offers a simple, interpretable, and deployable solution, applicable to routine H&E slides, that can guide treatment decisions and reduce unnecessary exposure in likely non-responders.

Although immune-activated tumors are often associated with improved outcomes, our survival analysis in TCGA data revealed that the prognostic value of TIME_ACT varies across cancer types. In the TCGA-SKCM cohort from which the TIME_ACT signature was originally derived, patients with TIME_ACT-High tumors demonstrated significantly improved overall survival compared to those with TIME_ACT-Low tumors (HR = 0.54, p = 8.2e−06) **(Extended Data Fig. 6a)**. A similar but modest association was observed in a pan-cancer analysis across all TCGA tumors after adjusting for cancer

type (HR = 0.86, p = 2e−05) **(Extended Data Fig. 6b)**. While this trend of better survival in TIME_ACT-High tumors was evident in multiple cancer types, statistically significant associations were limited to only a few **(Extended Data Fig. 6c)**. This finding should be interpreted with caution, as TCGA represents a heterogeneous collection of variably treated tumors, with incomplete annotation of treatment histories and other key clinical covariates. Moreover, immune activation may be more prominent in advanced or aggressive disease but not necessarily correlate with better prognosis in early-stage tumors, potentially confounding survival analyses. Overall, our results show that while TIME_ACT is a robust pan-cancer predictive biomarker of ICB response, its role as a prognostic indicator of patient survival merits further exploration.

This study has a few limitations. First, our analysis was retrospective in nature, and while the TIME_ACT score showed strong predictive performance across multiple cohorts and modalities, including both RNA-seq and slide-inferred expression data, prospective validation in clinical settings is called for. Second, while the current framework focuses on transcriptome-derived features, it does not incorporate histological or spatial characteristics of the tumor microenvironment. With the emergence of spatial slide-based gene expression inference, future efforts may explore integrating TIME_ACT with spatially resolved features to capture localized immune deserts, excluded regions, or inflamed niches that may be missed by conventional bulk RNA-seq [75,76]. Such integration could enhance the precision and applicability of TIME_ACT for guiding immunotherapy decisions in the clinic.

In summary, TIME_ACT is a biologically coherent, unsupervised transcriptomic signature biomarker of tumor immune activation, which robustly predicts ICB response across diverse tumor types via histology, thus offering an exciting potential for broad clinical utility. It thus lays a solid basis for further prospective studies to test its future use in the clinic as a first-of-its-kind, fast, cost-effective, and reliable ICB treatment biomarker.

Methods

Transcriptomic data acquisition and processing of raw RNA-seq data

Gene-expression and clinical data for The Cancer Genome Atlas (TCGA) and TARGET projects were obtained from the UCSC Xena portal [77] (last accessed 4 January 2025). Pre-processed STAR-aligned RNA-seq data ($\log_2$[count + 1]) for tumor samples in the TCGA Skin Cutaneous Melanoma (TCGA-SKCM) cohort were downloaded from the UCSC Xena data portal. For pan-cancer analyses, we retrieved RSEM-based, normalized RNA-seq data ($\log_2$[norm_count + 1]) for tumor samples from the TCGA + TARGET Pan-Cancer (PANCAN) cohort.

We selected publicly available anti-PD1-treated cohorts only if gene expression data were generated using RNA-seq experiments and clinical response annotations were available. Microarray-based datasets were excluded due to limited gene coverage and platform-specific biases that could compromise cross-cohort comparability. We have collected 15 anti-PD1 pre-treatment (total 943 patient samples) [44,50–64], 2 anti-PD1 on-treatment (total 74 patient samples) [50,51], and 1 anti-CTLA4 cohort (42 patient samples) [65]. Clinical response was uniformly defined using RECIST criteria [78], with complete response (CR) and partial response (PR) classified as responders, and stable disease (SD) and progressive disease (PD) as non-responders. To benchmark predictive performance, we compared TIME_ACT with other transcriptomic-based methods and immune-related gene signatures only in anti-PD1 datasets, as anti-PD1 therapy is the most widely used ICB treatment and has the largest number of publicly available RNA-seq cohorts suitable for consistent evaluation.

Gene-level TPM expression data were obtained where available directly from the GEO database or from supplementary materials provided by the respective publications. Several datasets were dbGaP-controlled, for which authorized access was obtained. Raw FASTQ files for these restricted-access cohorts were downloaded using the fasterq-dump utility (SRA Toolkit) with the provided dbGaP keys. Transcript abundance was quantified using Salmon [79] against the GENCODE GRCh38 reference transcriptome. Gene-level TPM values were then derived from transcript-level estimates using the tximport R package [80]. All TPM values were transformed to $\log_2(\text{TPM} + 1)$ prior to analysis. Single-cell gene expression data of melanoma patients were collected from the GSE115978 dataset [43].

Immune scoring-based classification of TCGA tumor samples

To assess the immune landscape of tumor samples, we utilized three independent immunophenotyping metrics: immune score, inflammatory response score, and number of tumor-infiltrating lymphocyte (TIL) patches. The Immune score of the TCGA samples was derived using the ESTIMATE algorithm [40]. The inflammatory response score of the TCGA samples was obtained from the Supplementary Data of Chen et al [41]. The Number of TIL patches per tumor sample was collected from Saltz et al. [42], which applied a deep learning-based image analysis pipeline to standard H&E-stained whole-slide images (WSIs) across the TCGA cohort to identify and quantify TIL-rich regions. These values were obtained directly from the publicly shared resource linked to the publication. For each metric, samples were ranked and dichotomized into immune-high (top 30%) and immune-low (bottom 30%) groups. To ensure stringent and biologically consistent classification, we defined “immune-active” (or “Hot”) tumors as those that fell within the top 30% for at least two out of the three scores and in none of the bottom 30%. Conversely, “immune-inactive” (or “Cold”) tumors were those in the bottom 30% for at least two scores and not in the top 30% for any. Samples not meeting these criteria were excluded from downstream binary comparisons to avoid intermediate or ambiguous immune phenotypes. This strict consensus-based approach enabled

the selection of only the true Hot and Cold tumors, serving as a high-confidence foundation for identifying a transcriptional signature of tumor immune activation or tumor hotness.

Differential expression analysis, pathway analysis, and derivation of TIME_ACT signature genes

To identify genes associated with tumor immune activation, we performed differential gene expression analysis using the limma package [81] between Hot (n = 66) and Cold (n = 49) tumors in the TCGA Skin Cutaneous Melanoma (TCGA-SKCM) cohort, as defined by the consensus-based immunophenotyping criteria described in the previous section. Genes were ranked by both moderated $\log_2$ fold change and B-statistic, the latter representing the log-odds of true differential expression under empirical Bayes moderation. Genes falling within the top 20th percentile for both metrics ($\log_2$FC > 3.66 and B > 48.5) were considered highly upregulated, resulting in a candidate set of 252 genes. Functional enrichment of these genes was conducted using the Enrichr platform [82], focusing on Gene Ontology (GO) Biological Process annotations. Significantly enriched pathways were identified based on adjusted p-values (Benjamini–Hochberg FDR < 0.05). Among the top 10 ranked GO terms, all were related to immune processes, including lymphocyte activation, T cell differentiation, and antigen presentation. Genes associated with these top ten immune-related categories were aggregated, yielding a final set of 66 genes, herein referred to as the TIME_ACT signature.

Weighted gene-co-expression network analysis

We applied WGCNA v1.73 [83] to the top 20,000 most variable genes in the TCGA-SKCM cohort to identify co-expression modules associated with the immune-hot phenotype. Samples were hierarchically clustered to detect outliers (cut height = 100), with none removed. A soft-thresholding power of 6 was selected based on the scale-free topology criterion ($R^2 > 0.8$). Using an unsigned topological overlap matrix (TOM), modules were detected via dynamic tree cutting. Module eigengenes were correlated with the Hot vs. Cold phenotype using Pearson correlation; the turquoise module showed the strongest positive association with immune-hot tumors. Gene centrality was quantified using module membership (kME), defined as the correlation between gene expression and the module eigengene. This allowed us to assess the topological importance of genes within each module and compare the distribution of kME values across gene sets, including the TIME_ACT signature genes.

Single-sample gene-set enrichment (ssGSEA) analysis

Log-transformed TPM values ($\log_2$(TPM + 1)) were first converted to gene-wise z-scores to remove between-gene baseline differences and residual library-size effects. This transformation ensures that highly expressed housekeeping genes do not disproportionately influence the within-sample ranking that underlies ssGSEA. Enrichment of TIME_ACT and comparator signatures was then quantified using the

GSVA package (v2.0.7) [84] in ssGSEA mode in R v4.4.3. The analysis was performed with alpha = 0, which assigns equal weight to all ranked positions, yielding an enrichment score that reflects the overall representation of signature genes across the expression rank, rather than emphasizing only the most highly expressed genes. The parameter normalize = TRUE was applied to rescale the scores to the range [–1, 1], enabling consistent comparisons across samples and tumor types.

Spatial and Single-cell analysis of TIME_ACT signature genes

To investigate the spatial immune architecture, we analyzed two breast cancer tissue sections, formalin-fixed paraffin-embedded (FFPE) and fresh-frozen (FF), obtained from the 10x Genomics public dataset repository (https://www.10xgenomics.com/datasets). The FF tissue corresponded to HER2-positive, while the FFPE specimen displayed histological heterogeneity characterized by distinct regions of Ductal Carcinoma In Situ (DCIS) and invasive carcinoma of undetermined molecular subtype. Both tissue sections were accompanied by spot-level histopathological annotations provided by expert pathologists to categorize cellular components into tumor cells, stromal cells, lymphocytes, and macrophages. TIME_ACT scores were calculated for each individual spot, with spots exceeding the threshold of 0.0655 classified as "Hot" regions. Subsequently, spatial visualization maps were generated by overlaying pathologist-annotated cellular phenotypes with TIME_ACT-hot regions onto their corresponding tissue sections.

Further, to perform the spatial proximity analysis, we utilized digital pathology annotations that were manually curated by expert pathologists available in the PanopTILS (https://sites.google.com/view/panoptils/) resource [46,47]. Specifically, we used the regions of interest (ROIs) provided for breast cancer patients from the TCGA dataset to investigate the spatial relationships between cancer cells, stromal cells, and tumor-infiltrating lymphocytes (TILs). Cell centroid coordinates were calculated either from the provided coordinates. Using these centroids, pairwise spatial distances between cells in each defined group were computed via the Euclidean distance metric. Several key metrics were derived, including mean nearest neighbor distances (NND) from cancer and stromal cells to lymphocytes, fractions of cancer cells and stromal cells with lymphocytes within a 150-pixel radius, and fractions of cancer cells having stromal cells within a 150-pixel radius. Data was aggregated per patient by calculating mean metrics across multiple ROIs, resulting in robust patient-level spatial proximity features. Subsequently, correlations between these spatial metrics and TIME_ACT scores were assessed using Spearman correlation. Analyses were restricted to patients with complete and valid spatial data. Statistical significance was evaluated, with p-values reported alongside Spearman correlation coefficients. All these data preprocessing and computational analyses were performed using a customized Python-based pipeline (version 3.12). The workflow integrated Pandas (2.2.2) for efficient data handling, NumPy (1.24.4) for numerical computations, Matplotlib (3.7.2) for high-resolution spatial

visualization, Pillow (9.2.0) for processing large-scale histological images, and SciPy (cdist and spearmanr) for spatial distance computations and correlation analyses.

We obtained single-cell RNA-seq data from the GEO database (accession GSE115978), generated using the Smart-seq2 protocol on fresh tumor resections from 31 melanoma patients. The count matrix and accompanying metadata were imported into R and converted into a Seurat object. To compute cell-type–specific expression, we used Seurat's "AverageExpression" function to calculate the mean log-TPM value of each gene within each annotated cell type. To mitigate inter-patient variability, we first calculated these cell-type–specific values for each patient individually and then averaged them across all patients for each gene and cell type. The resulting averaged expression matrix was visualized as a heatmap using the pheatmap package in R. Additionally, TIME_ACT gene expression patterns were retrieved from diverse single-cell RNA-seq datasets across multiple cancer types, as curated in the TISCH2 database [85].

Predictive performance evaluation, threshold optimization, and statistical analysis

To evaluate the predictive performance of TIME_ACT, alongside comparator gene signatures and transcriptomic-based approaches, in stratifying responders from non-responders to immune checkpoint blockade (ICB) and other therapies, we computed the area under the receiver operating characteristic curve (AUC), area under the precision-recall curve (AUPRC) and the odds ratio (OR). AUC values were calculated using the roc_auc_score function, and AUPRC values were obtained using the average_precision_score function from the scikit-learn package (v1.4.2) [86] in Python 3.12, providing a threshold-independent measure of classification accuracy. A one-sided paired Wilcoxon signed-rank test was used to compare AUC values of TIME_ACT against each signature and method across cohorts. To define a consistent classification threshold for pan-cancer TIME_ACT stratification, we applied Youden's index [87] (J = Sensitivity + Specificity – 1) across nine TCGA cancer types using predefined Hot and Cold tumor labels. The TIME_ACT score that maximized Youden's index was selected as the optimal pan-cancer decision threshold (0.0655). This threshold was then applied uniformly across all external validation cohorts to classify samples as TIME_ACT-high or TIME_ACT-low and to compute odds ratios for treatment response. All additional statistical analyses, including Pearson correlation and multiple hypothesis testing (Benjamini–Hochberg false discovery rate), were performed in R v4.4.3.

Clinical Histopathology Cohorts

To evaluate the TIME_ACT signature in real-world clinical settings, we curated a multi-institutional collection of new and unpublished clinical histopathology datasets encompassing whole-slide H&E-stained tumor sections alongside detailed treatment annotations and clinical outcomes. In total, we collected eight cohorts from seven cancer types, each with annotated treatment information and clinical response to therapy. One additional dataset was received that did not include treatment response

information; only overall survival data were available for the patients. We received slides and metadata with variable levels of detail and formatting. Across all datasets, we only retained slides from patients who received ICB as part of their treatment regimen. Here is the description of each cohort that we analyzed.

1. ***NCI Bladder Cancer (urothelial carcinoma) cohort:*** The NCI bladder cancer (BLCA) cohort included 48 patients (48 slides) with locally advanced or metastatic urothelial carcinoma of the bladder. This was a subset of a larger trial (NCT02496208) that enrolled 150 patients across multiple metastatic genitourinary tumors (GU) [88,89]. All the BLCA patients included in our analysis were treated with cabozantinib and nivolumab alone or with ipilimumab. All slides were archival pre-treatment FFPE specimens. In total, 17 patients responded to therapy and 31 did not.
2. ***Cedars-Sinai Melanoma (SKCM) cohort:*** This cohort comprised 35 patients with advanced melanoma (35 slides). All patients were treated with ICB regimens. Treatments included anti-PD-1 monotherapy in some cases and various combination immunotherapies - for example, PD-1 inhibitors combined with CTLA-4 blockade (ipilimumab + nivolumab), with LAG-3 blockade, or with other investigational immunomodulators (such as an IDO1 inhibitor or GITR agonist) - reflecting the clinical trial therapies used. There were 21 responders and 14 non-responders in this melanoma cohort.
3. ***Cedars-Sinai Breast Cancer (BRCA) cohort***: This cohort included a total of 23 tumor slides, derived from the Cedars-Sinai "Molecular Twin Research Umbrella Protocol" (IRB STUDY00001879). All patients had advanced invasive breast carcinoma and were treated with ICB (anti-PD-1/PD-L1 therapy). Of the 23 samples, 15 were annotated as responders and 8 as non-responders. In the responder group, 11 were treated with a combination of ICB and chemotherapy, and four patients received a combination of immunotherapy (pembrolizumab and trastuzumab) and supportive chemotherapy. In the non-responder group, 6 received ICB and chemotherapy (in one patient, chemotherapy, ICB, and trastuzumab), and two received ICB therapy alone. H&E slides were derived from surgical FFPE specimens collected between January 2013 and July 2024.
4. ***Cedars-Sinai Lung Adenocarcinoma (LUAD) cohort:*** The Cedars-Sinai LUAD cohort consisted of 30 patients (30 slides in total), all with KRAS-mutant lung adenocarcinoma. All patients had stage IV or recurrent lung adenocarcinoma and received ICB, either alone or in combination with chemotherapy. The majority (24/30) were treated with first-line platinum-based chemotherapy plus anti-PD-1 immunotherapy, while 6 patients received immunotherapy alone. 14 patients were responders, and 16 patients were non-responders. All slides were derived from surgical FFPE specimens.
5. ***HCRN Renal Cell Carcinoma cohort:*** This cohort included 96 patients with metastatic clear cell renal cell carcinoma (KIRC; 151 pre-treatment tumor slides) and 28 patients with advanced papillary renal cell carcinoma (KIRP; 48 pre-treatment tumor slides). All patients were enrolled in the HCRN GU16-260 clinical trial (NCT03117309) and received nivolumab monotherapy [90–92]. Multiple patients

contributed paired specimens from primary and metastatic sites. Among the KIRC patients, 35 responded to therapy and 61 did not. Among the KIRP patients, 4 were responders and 24 were non-responders. All slides were derived from FFPE tissue blocks. A subset of KIRC de-identified RNA-seq data [93], linked to histopathology and clinical outcome, was retrieved through dbGaP (phs003618.v1.p1).

6. ***Taiwan NYCU Head and Neck Squamous Cell Carcinoma cohort 1 (Taiwan-HNSCC$_1$):*** The Taiwan-HNSCC$_1$ cohort was prospectively collected under the project of National Science and Technology Council, Taiwan. This cohort includes 33 HNSCC patient slides, among whom 11 were classified as responders to immunotherapy and 22 as non-responders. Among responders, 8 received ICB monotherapy, 2 received ICB with chemotherapy, and 1 received ICB with targeted therapy. Among non-responders, 5 received ICB monotherapy, 11 received ICB with chemotherapy, 5 received ICB with targeted therapy, and 1 received the full combination.
7. ***Taiwan NYCU Head and Neck Squamous Cell Carcinoma cohort 2 (Taiwan-HNSCC$_2$):*** The Taiwan-HNSCC$_2$ cohort was retrospectively collected from the Big Data Center of Taipei Veterans General Hospital. Cohort 2 includes another 62 HNSCC patient slides. Within this cohort, 21 patients were identified as responders, and 41 as non-responders. Among responders, 5 received ICB monotherapy, 8 received ICB with chemotherapy, 2 received ICB with targeted therapy, and 6 received the full combination. In the non-responder group, 19 received ICB monotherapy, 14 received ICB with chemotherapy, 5 received ICB with targeted therapy, and 3 received the full combination. We used 61 slides, not included one non-responder patient slide due to poor image quality.
8. ***Sheba Medical Center Lung Squamous Cell Carcinoma cohort:*** The Sheba Medical Center Lung Squamous Cell Carcinoma (LUSC) cohort included 62 patients (71 slides) who were treated with ICB, along with other treatments. However, response information based on RECIST criteria was not recorded for this cohort; only overall survival data were available.

Inferring gene expression from histopathology images using Path2Omics

We utilized our recently developed Path2Omics pipeline [36] to infer gene expression profiles directly from pathology slide images. Briefly, Path2Omics consists of three main components: image pre-processing, feature extraction, and regression. Initially, whole slide images were divided into non-overlapping tiles of 512 by 512 RGB pixels and then underwent color normalization. For feature extraction, a foundational model pre-trained on digital pathology data was used to derive informative features from each tile. These features were then input into a multi-layer perceptron within the regression module to predict gene expression values. Path2Omics was initially trained and cross-validated on the TCGA dataset separately for each cancer type. The pre-trained models were subsequently applied to predict gene expression from slides on the clinical treatment datasets, without additional training. The methodological details are provided in the original manuscript [36].

Data availability

TCGA data are publicly available at the Genomic Data Commons Data Portal (https://portal.gdc.cancer.gov). The accession IDs of the ICB transcriptomic cohorts used in this study are provided in Extended Data Table 6. Requests for access to unpublished data from eight clinical histopathology cohorts should be directed to the corresponding authors. Each request will be assessed individually within 15 business days to ensure adherence to intellectual property rights and patient privacy standards.

Code availability

The code supporting this publication will be made available for academic research purposes via: (https://zenodo.org/records/15712666). Any additional information is available from the corresponding authors upon request.

Acknowledgements

This research is supported in part by the Intramural Research Program of the National Institutes of Health, National Cancer Institute, Center for Cancer Research. This work has utilized the computational resources of the NIH HPC Biowulf cluster (http://hpc.nih.gov). We thank the Cedars-Sinai Medical Center OncoBiobank and Pathology Shared Resources for their technical assistance. We also thank the Big Data Center of Taipei Veterans General Hospital for their help in data sharing. The results presented are in part based on the data generated by the Cancer Genome Atlas Research Network (https://www.cancer.gov/tcga/). We would additionally like to acknowledge Nicholas P. Restifo, Nishanth Ulhas Nair, Sanna Madan, and Alejandro Schaffer for helpful discussions, and the members of the Cancer Data Science Laboratory for their constructive feedback. ChatGPT v4o (https://chatgpt.com/) was used strictly to refine certain existing paragraphs to improve sentence constructions. The biorender (https://www.biorender.com/) licensed version was used to generate some panels of Figure 1.

Competing interest

E.R. is a co-founder of Medaware, Metabomed, and Pangea Biomed (divested from the latter). E.R. serves as a non-paid scientific consultant to Pangea Biomed under a collaboration agreement between Pangea Biomed and the NCI. E.R. also serves as a scientific advisory board member of GSK Oncology and the ProCan project. The other authors declare no competing interests.

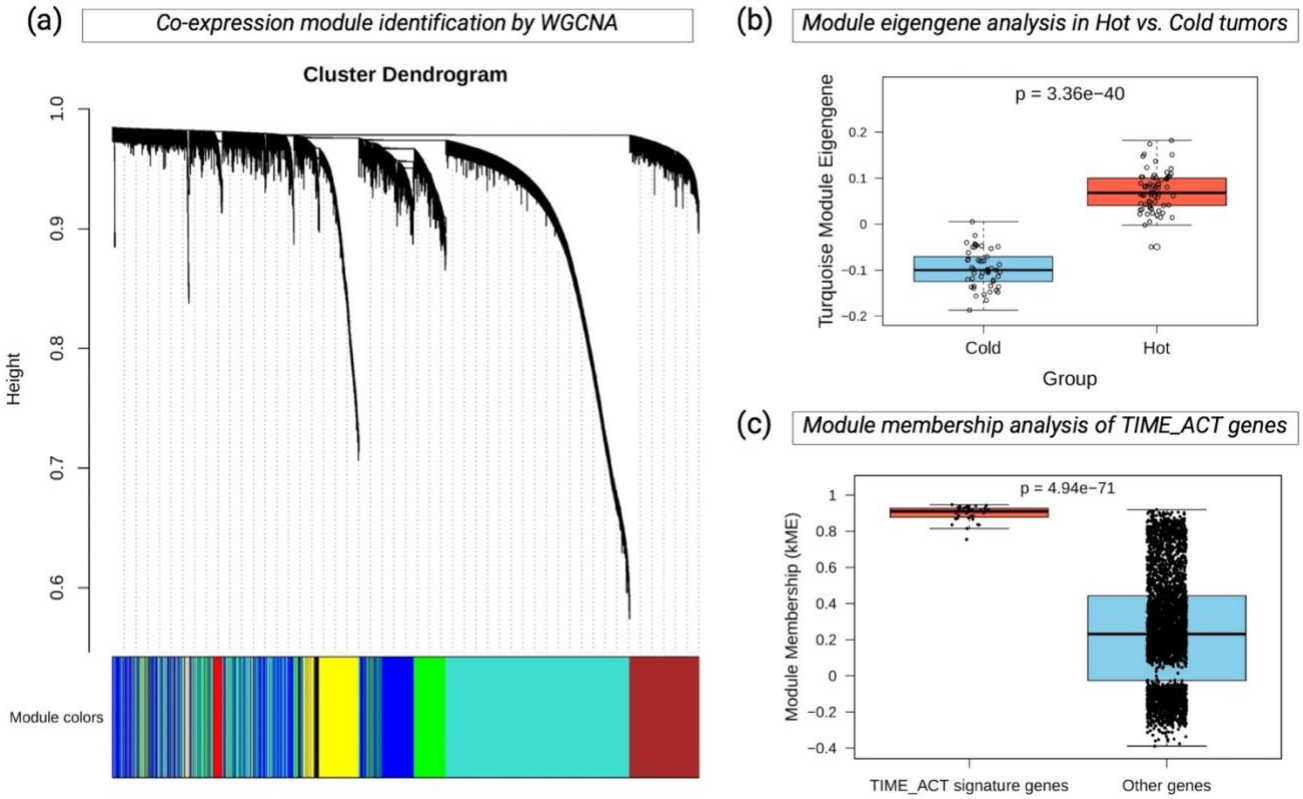

Extended Data Fig. 1 | Weighted Gene Co-expression Network Analysis (WGCNA) identifies a TIME_ACT-associated gene module in melanoma. **(a)** Hierarchical clustering dendrogram of genes from TCGA melanoma tumors grouped into distinct co-expression modules by WGCNA. Each color in the horizontal bar represents a different gene module. The turquoise module, highlighted in the plot, contains all 66 genes from the TIME_ACT signature, indicating that they are tightly co-expressed within a single immune-related network module. **(b)** Boxplot comparing the eigengene values of the turquoise module between cold and hot tumors. The turquoise module shows significantly higher expression in hot tumors (p = 3.36e 40), indicating a strong association with immunologically active TIME. **(c)** Module membership (kME) scores comparing TIME_ACT signature genes vs. all other genes within the turquoise module. TIME_ACT genes exhibit significantly stronger module membership (p = 4.94e–71), highlighting their central role in the hot immune phenotype co-expression network.

Extended Data Fig. 2 | TIME_ACT genes are consistently expressed in immune cell populations across multiple cancer types at single-cell resolution. Cell-type-specific expression of TIME_ACT genes was assessed using eight annotated single-cell RNA-seq datasets from the TISCH2 database. **(a-h)** UMAP plots and gene expression heatmaps demonstrate consistent enrichment of TIME_ACT gene expression in immune compartments, particularly $CD8^+$ T cells, $CD4^+$ T cells, B cells, and dendritic cells, across lung cancer, breast cancer, liver cancer, and other tumor types. Minimal or no expression was observed in malignant cells, fibroblasts, or endothelial cells. These findings validate the immune cell

specificity of the TIME_ACT signature and reinforce its relevance as a marker of functional immune engagement across diverse TME.

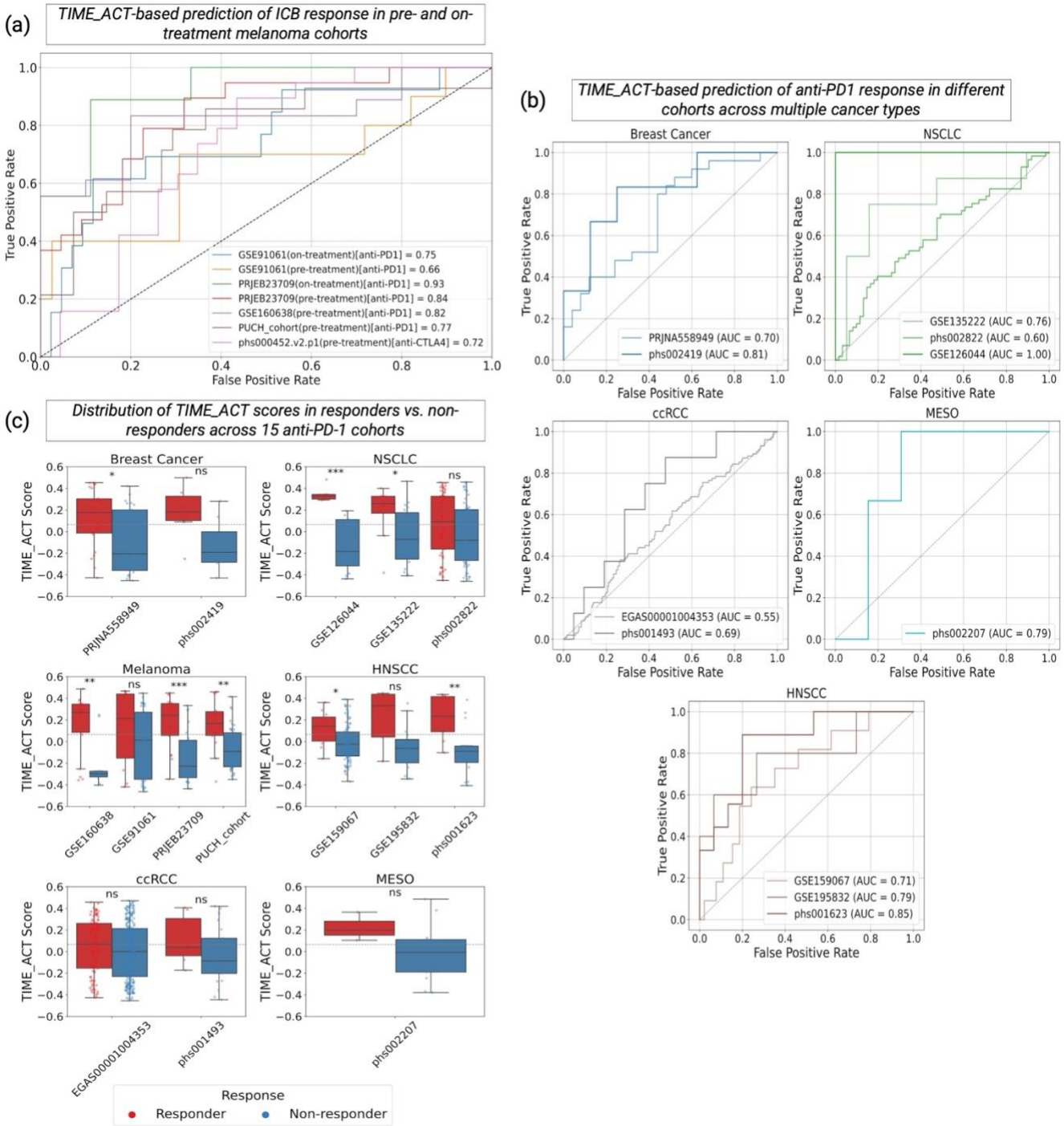

Extended Data Fig. 3 | TIME_ACT robustly predicts ICB response across pre- and on-treatment transcriptomic datasets from melanoma and other cancers. **(a)** TIME_ACT scores stratify responders and non-responders in five melanoma cohorts with available response annotations. These include four anti-PD-1-treated cohorts- GSE160638, PUCH, GSE91061 (pre- and on-treatment), PRJEB23709 (pre- and on-treatment), and one anti-CTLA-4-treated cohort (phs000452). Notably, prediction accuracy improves in on-treatment samples compared to pre-treatment samples (e.g., AUC =

0.93 for PRJEB23709 on-treatment vs. AUC = 0.84 pre-treatment), indicating that TIME_ACT captures both baseline immune activation and early therapy-induced changes. **(b)** ROC curves summarizing TIME_ACT performance in anti-PD1-treated non-melanoma pre-treatment cohorts across five cancer types: breast cancer, non–small cell lung cancer (NSCLC), head and neck squamous cell carcinoma (HNSCC), renal cell carcinoma (ccRCC), and mesothelioma. TIME_ACT achieved strong predictive accuracy across these datasets, supporting its pan-cancer generalizability. **(c)** Distribution of TIME_ACT scores in responders versus non-responders across all 15 anti-PD1 cohorts. Responders consistently display significantly higher TIME_ACT scores, underscoring the predictive value of the signature in clinically relevant settings.

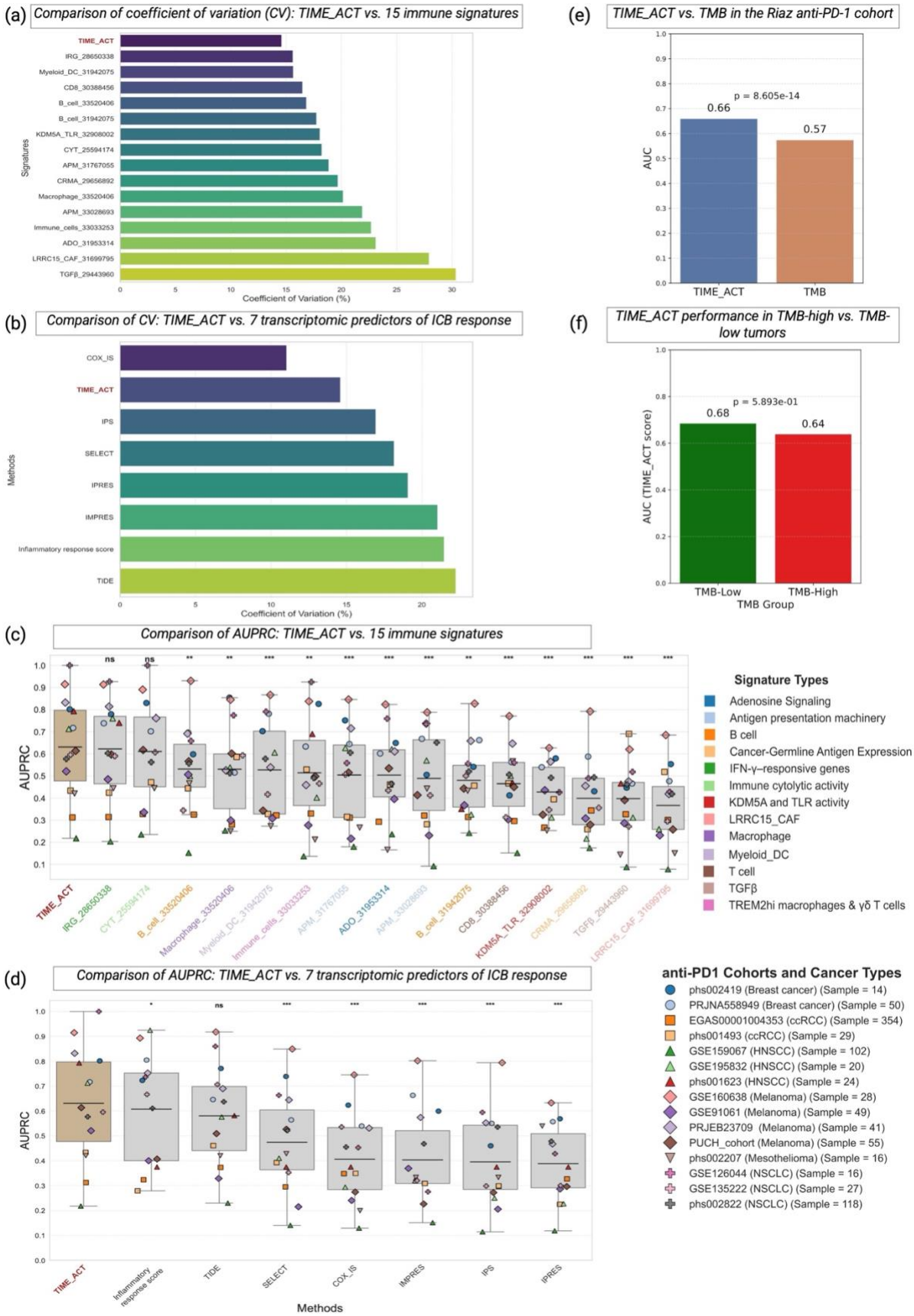
(a)
Comparison of coefficient of variation (CV): TIME_ACT vs. 15 immune signatures
TIME_ACT
IRG_28650338
Myeloid_DC_31942075
CD8_30388456
B_cell_33520406
B_cell_31942075
KDM5A_TLR_32908002
CYT_25594174
APM_31767055
CRMA_29656892
Macrophage_33520406
APM_33028693
Immune_cells_33033253
ADO_31953314
LRRC15_CAF_31699795
TGFβ_29443960
Signatures
Coefficient of Variation (%)
(b)
Comparison of CV: TIME_ACT vs. 7 transcriptomic predictors of ICB response
COX_IS
TIME_ACT
IPS
SELECT
IPRES
IMPRES
Inflammatory response score
TIDE
Methods
Coefficient of Variation (%)
(c)
Comparison of AUPRC: TIME_ACT vs. 15 immune signatures
AUPRC
Signature Types
Adenosine Signaling
Antigen presentation machinery
B cell
Cancer-Germline Antigen Expression
IFN-γ–responsive genes
Immune cytolytic activity
KDM5A and TLR activity
LRRC15_CAF
Macrophage
Myeloid_DC
T cell
TGFβ
TREM2hi macrophages & γδ T cells
(d)
Comparison of AUPRC: TIME_ACT vs. 7 transcriptomic predictors of ICB response
AUPRC
TIME_ACT
Inflammatory response score
TIDE
SELECT
COX_IS
IMPRES
IPS
IPRES
Methods
anti-PD1 Cohorts and Cancer Types
phs002419 (Breast cancer) (Sample = 14)
PRJNA558949 (Breast cancer) (Sample = 50)
EGAS00001004353 (ccRCC) (Sample = 354)
phs001493 (ccRCC) (Sample = 29)
GSE159067 (HNSCC) (Sample = 102)
GSE195832 (HNSCC) (Sample = 20)
phs001623 (HNSCC) (Sample = 24)
GSE160638 (Melanoma) (Sample = 28)
GSE91061 (Melanoma) (Sample = 49)
PRJEB23709 (Melanoma) (Sample = 41)
PUCH_cohort (Melanoma) (Sample = 55)
phs002207 (Mesothelioma) (Sample = 16)
GSE126044 (NSCLC) (Sample = 16)
GSE135222 (NSCLC) (Sample = 27)
phs002822 (NSCLC) (Sample = 118)
(e)
TIME_ACT vs. TMB in the Riaz anti-PD-1 cohort
p = 8.605e-14
0.66
0.57
AUC
TIME_ACT
TMB
(f)
TIME_ACT performance in TMB-high vs. TMB-low tumors
p = 5.893e-01
0.68
0.64
AUC (TIME_ACT score)
TMB-Low
TMB-High
TMB Group

Extended Data Fig. 4 | Benchmarking TIME_ACT against immune-related signatures, transcriptomic methods, and TMB in predicting ICB response. **(a)** Coefficient of variation (CV) of AUC across cohorts for each immune-related signature. TIME_ACT exhibits the lowest inter-cohort variability, supporting its robustness. **(b)** CV of AUC across the 7 transcriptomic methods shows TIME_ACT maintains consistent performance across heterogeneous datasets. **(c)** Comparison of the area under the precision-recall curve (AUPRC) between TIME_ACT and 15 immune-related gene expression signatures across 15 anti-PD1 cohorts. TIME_ACT demonstrates the highest AUPRC across all datasets, indicating superior ability to correctly identify responders. Statistical significance for the comparison of TIME_ACT with each signature was calculated using a one-sided Wilcoxon signed-rank test ($p < 0.05$ = *, $p < 0.01$ = **, $p < 0.001$ = ***). **(d)** Benchmarking AUPRC of TIME_ACT against 7 widely used transcriptomic-based prediction methods (e.g., TIDE, IMPRES, SELECT). TIME_ACT again achieves the highest AUPRC, suggesting robust classification performance. **(e)** In the Riaz et al. melanoma cohort with matched RNA-seq and TMB data, TIME_ACT (AUC = 0.66) outperforms TMB (AUC = 0.57) in predicting ICB response. **(f)** TIME_ACT retains predictive power in both TMB-High (AUC = 0.64) and TMB-Low (AUC = 0.68) tumors, demonstrating its utility in genomic biomarker-poor settings where TMB fails to stratify responders.

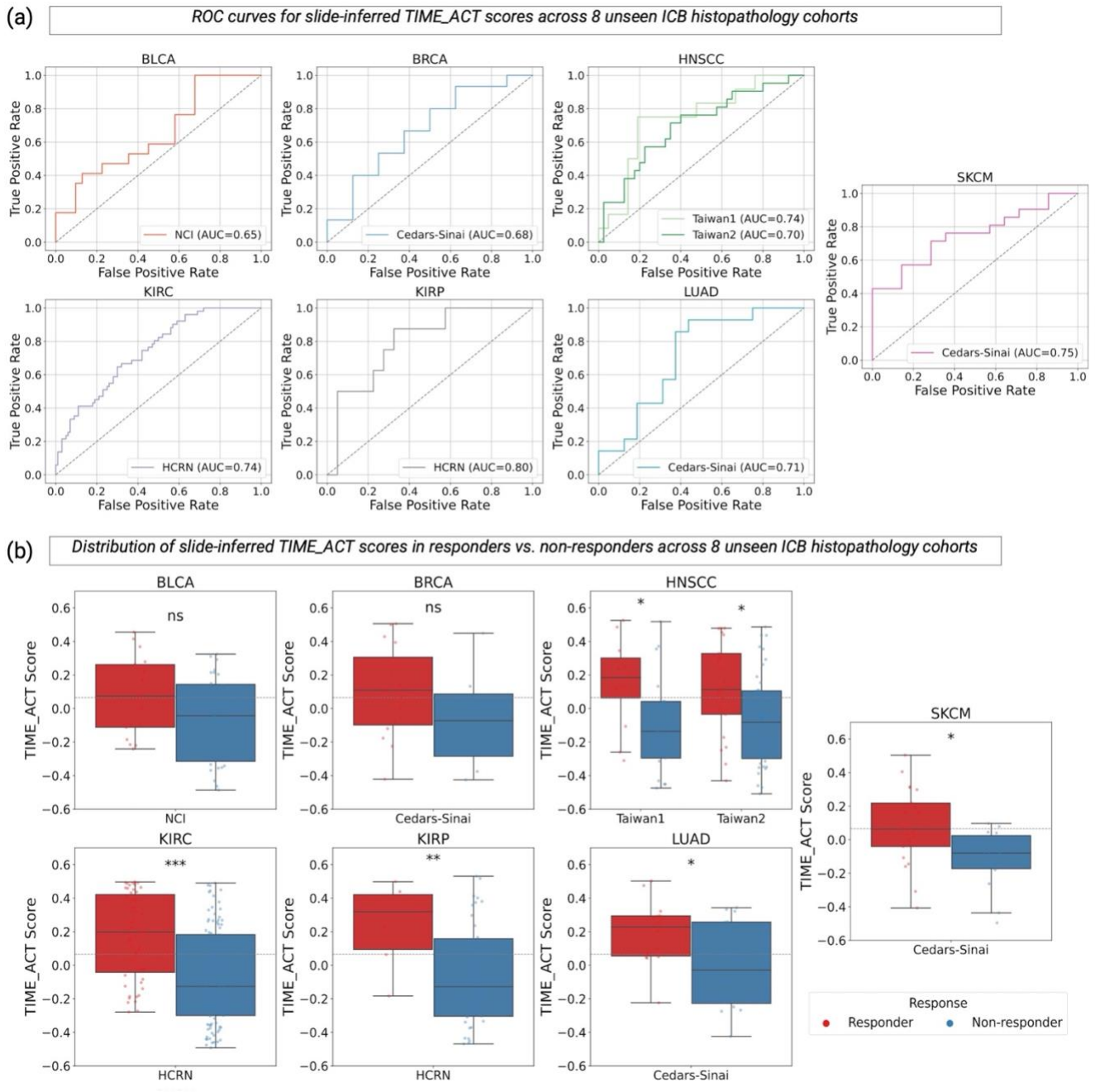

Extended Data Fig. 5 | TIME_ACT scores inferred from histopathology predict ICB response across 8 unseen cohorts. **(a)** ROC curves evaluating the predictive performance of slide-inferred TIME_ACT scores in eight independent ICB-treated cohorts. TIME_ACT scores were computed using gene expression inferred from diagnostic H&E slides via the Path2Omics model. AUC values ranged from 0.65 to 0.80, with a mean AUC of 0.72, indicating consistent predictive performance across cancer types and institutions. **(b)** Box plots showing the distribution of slide-inferred TIME_ACT scores in responders versus non-responders. In all eight cohorts, responders exhibit significantly higher inferred TIME_ACT scores, reinforcing the translational relevance of histology-based immune activation prediction for clinical decision-making.

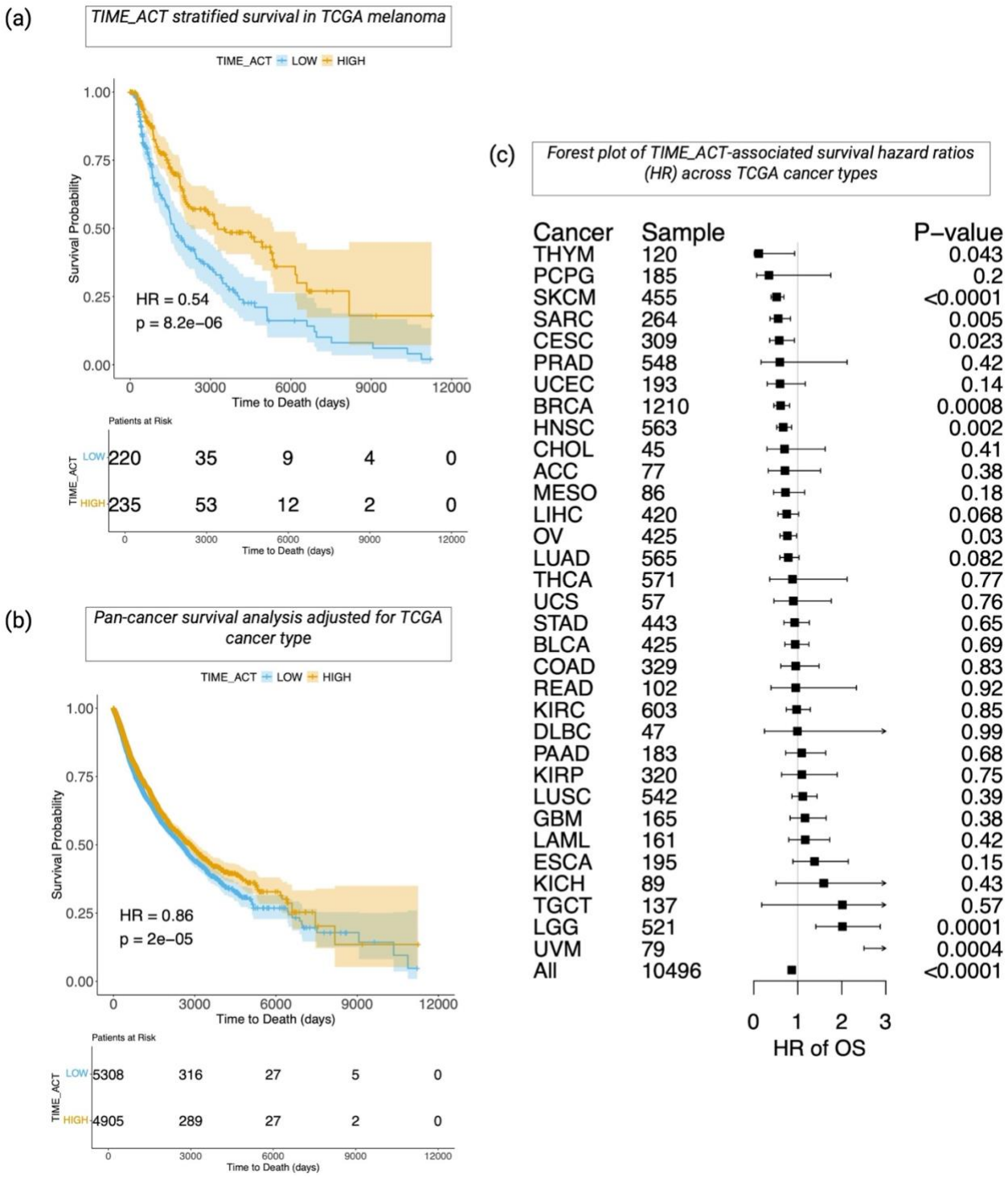

Extended Data Fig. 6 | Associations between TIME_ACT scores and overall survival across TCGA cancers. **(a)** Kaplan-Meier (K-M) survival analysis of TCGA-SKCM patients stratified by TIME_ACT score using the pan-cancer threshold (0.0655). TIME_ACT-High tumors show significantly improved overall survival compared to TIME_ACT-Low tumors (hazard ratio = 0.54, p = 8.2e-06). **(b)** Pan-cancer survival analysis of all TCGA tumors, adjusted for cancer type, reveals a modest but significant association between high TIME_ACT scores and better overall survival (HR = 0.86, p = 2e−05). **(c)** Forest plot of

hazard ratios for overall survival across 33 individual TCGA cancer types. While a favorable trend is observed in most tumor types, statistically significant associations ($p < 0.05$) are observed only in a subset (e.g., SKCM, BRCA, HNSC), emphasizing that the prognostic utility of TIME_ACT is context-dependent and not universally predictive of survival across all cancers.

Extended Data Tables Descriptions

Extended Data Table 1 | Differentially expressed genes between immune-hot and immune-cold TCGA melanoma samples. This table lists the 252 genes significantly upregulated in TIME_ACT-defined immune-hot tumors versus cold tumors in the TCGA-SKCM cohort, identified using limma with stringent thresholds on both $\log_2$ fold change (logFC > 3.66) and B-statistic (B > 48.5). Includes gene identifiers, average expression, t-statistics, p-values, adjusted p-values, and B-statistics.

Extended Data Table 2 | Gene ontology enrichment analysis of genes upregulated in immune-hot tumors. Enriched immune-related biological processes among the 252 upregulated genes in TIME_ACT-hot tumors. Columns include GO term name, adjusted p-value, odds ratio, and combined enrichment score from Enrichr.

Extended Data Table 3 | The TIME_ACT 66-gene immune activation signature. List of 66 genes forming the TIME_ACT signature, derived from genes upregulated in immune-hot tumors and involved in top-ranked immune-related GO terms.

Extended Data Table 4 | TIME_ACT scores and immune activation annotations across annotated TCGA cohorts. TIME_ACT scores and their associated Hot/Cold immune annotations for TCGA samples from the 9 tumor types. Includes sample ID, TIME_ACT score, annotation, and cancer type.

Extended Data Table 5 | TIME_ACT scores across all TCGA tumors. Pan-cancer TIME_ACT scores computed for all TCGA tumor samples using ssGSEA. This table provides sample ID, TIME_ACT score, and tumor type.

Extended Data Table 6 |Summary of pre-treatment anti-PD1 transcriptomic cohorts used in this study. Overview of the 15 anti-PD1-treated transcriptomic datasets used to assess the predictive performance of TIME_ACT and to compare it with other signatures and methods. Includes cohort name, cancer type, total sample size, number of responders, and non-responders.

Extended Data Table 7 | List of comparator immune-related gene expression signatures used for benchmarking. Details of 15 established immune-related transcriptomic signatures used for benchmarking TIME_ACT. Includes signature name, type, PubMed ID (PMID), and gene list for each signature.

References

1. Liu, Y. *et al.* Predicting patient outcomes after treatment with immune checkpoint blockade: A review of biomarkers derived from diverse data modalities. *Cell Genomics* vol. 4 Preprint at https://doi.org/10.1016/j.xgen.2023.100444 (2024).
2. Sun, Q. *et al.* Immune checkpoint therapy for solid tumours: clinical dilemmas and future trends. *Signal Transduction and Targeted Therapy* vol. 8 Preprint at https://doi.org/10.1038/s41392-023-01522-4 (2023).
3. Lei, Y., Li, X., Huang, Q., Zheng, X. & Liu, M. Progress and Challenges of Predictive Biomarkers for Immune Checkpoint Blockade. *Frontiers in Oncology* vol. 11 Preprint at https://doi.org/10.3389/fonc.2021.617335 (2021).
4. McGrail, D. J. *et al.* High tumor mutation burden fails to predict immune checkpoint blockade response across all cancer types. *Annals of Oncology* **32**, (2021).
5. Gurjao, C., Tsukrov, D., Imakaev, M., Luquette, L. J. & Mirny, L. A. Is tumor mutational burden predictive of response to immunotherapy? *Elife* **12**, (2023).
6. Ren, X. *et al.* Immunological Classification of Tumor Types and Advances in Precision Combination Immunotherapy. *Frontiers in Immunology* vol. 13 Preprint at https://doi.org/10.3389/fimmu.2022.790113 (2022).
7. Zhang, J., Huang, D., Saw, P. E. & Song, E. Turning cold tumors hot: from molecular mechanisms to clinical applications. *Trends in Immunology* vol. 43 Preprint at https://doi.org/10.1016/j.it.2022.04.010 (2022).
8. Cottrell, T. R. *et al.* Society for Immunotherapy of Cancer (SITC) consensus statement on essential biomarkers for immunotherapy clinical protocols. *J Immunother Cancer* **13**, (2025).
9. Zhang, J., Shi, Z., Xu, X., Yu, Z. & Mi, J. The influence of microenvironment on tumor immunotherapy. *FEBS Journal* vol. 286 Preprint at https://doi.org/10.1111/febs.15028 (2019).
10. Zhou, C., Liu, Q., Xiang, Y., Gou, X. & Li, W. Role of the tumor immune microenvironment in tumor immunotherapy (Review). *Oncology Letters* vol. 23 Preprint at https://doi.org/10.3892/ol.2021.13171 (2022).
11. Petitprez, F., Meylan, M., de Reyniès, A., Sautès-Fridman, C. & Fridman, W. H. The Tumor Microenvironment in the Response to Immune Checkpoint Blockade Therapies. *Frontiers in Immunology* vol. 11 Preprint at https://doi.org/10.3389/fimmu.2020.00784 (2020).
12. Wang, L. *et al.* Hot and cold tumors: Immunological features and the therapeutic strategies. *MedComm* vol. 4 Preprint at https://doi.org/10.1002/mco2.343 (2023).
13. Huang, H. *et al.* T cell proliferation-related genes: Predicting prognosis, identifying the cold and hot tumors, and guiding treatment in clear cell renal cell carcinoma. *Front Genet* **13**, (2022).
14. Xiong, X. *et al.* Identification of a novel defined inflammation-related long noncoding RNA signature contributes to predicting prognosis and distinction between the cold and hot tumors in bladder cancer. *Front Oncol* **13**, (2023).
15. Hao, C. *et al.* Predicting prognosis, immunotherapy and distinguishing cold and hot tumors in clear cell renal cell carcinoma based on anoikis-related lncRNAs. *Front Immunol* **14**, (2023).
16. Ren, C. *et al.* Metabolic syndrome-related prognostic index: Predicting biochemical recurrence and differentiating between cold and hot tumors in prostate cancer. *Front Endocrinol (Lausanne)* **14**, (2023).
17. He, R. *et al.* Identification of RNA Methylation-Related lncRNAs Signature for Predicting Hot and Cold Tumors and Prognosis in Colon Cancer. *Front Genet* **13**, (2022).
18. Liu, D. *et al.* Predicting Prognosis and Distinguishing Cold and Hot Tumors in Bladder Urothelial Carcinoma Based on Necroptosis-Associated lncRNAs. *Front Immunol* **13**, (2022).
19. Zhang, M. *et al.* Comprehensive prediction of immune microenvironment and hot and cold tumor differentiation in cutaneous melanoma based on necroptosis-related lncRNA. *Sci Rep* **13**, (2023).
20. Ayers, M. *et al.* IFN-γ-related mRNA profile predicts clinical response to PD-1 blockade. *Journal of Clinical Investigation* **127**, (2017).
21. Sade-Feldman, M. *et al.* Defining T Cell States Associated with Response to Checkpoint Immunotherapy in Melanoma. *Cell* **175**, (2018).
22. Wang, B. *et al.* Decoupling the correlation between cytotoxic and exhausted T lymphocyte states enhances melanoma immunotherapy response prediction. *iScience* **27**, (2024).
23. Helmink, B. A. *et al.* B cells and tertiary lymphoid structures promote immunotherapy response. *Nature* **577**, (2020).
24. Budczies, J. *et al.* A gene expression signature associated with B cells predicts benefit from immune checkpoint blockade in lung adenocarcinoma. *Oncoimmunology* **10**, (2021).

25. Wang, S., He, Z., Wang, X., Li, H. & Liu, X. S. Antigen presentation and tumor immunogenicity in cancer immunotherapy response prediction. *Elife* **8**, (2019).
26. Thompson, J. C. *et al.* Gene signature of antigen processing and presentation machinery predicts response to checkpoint blockade in non-small cell lung cancer (NSCLC) and melanoma. *J Immunother Cancer* **8**, (2020).
27. Jiang, P. *et al.* Signatures of T cell dysfunction and exclusion predict cancer immunotherapy response. *Nat Med* **24**, (2018).
28. Auslander, N. *et al.* Robust prediction of response to immune checkpoint blockade therapy in metastatic melanoma. *Nat Med* **24**, (2018).
29. Lee, J. S. *et al.* Synthetic lethality-mediated precision oncology via the tumor transcriptome. *Cell* **184**, (2021).
30. Hugo, W. *et al.* Genomic and Transcriptomic Features of Response to Anti-PD-1 Therapy in Metastatic Melanoma. *Cell* **165**, (2016).
31. A Set of Transcriptomic Changes Is Associated with Anti-PD-1 Resistance. *Cancer discovery* vol. 6 Preprint at https://doi.org/10.1158/2159-8290.CD-RW2016-057 (2016).
32. Charoentong, P. *et al.* Pan-cancer Immunogenomic Analyses Reveal Genotype-Immunophenotype Relationships and Predictors of Response to Checkpoint Blockade. *Cell Rep* **18**, (2017).
33. Bonavita, E. *et al.* Antagonistic Inflammatory Phenotypes Dictate Tumor Fate and Response to Immune Checkpoint Blockade. *Immunity* **53**, (2020).
34. Kang, H. *et al.* A Comprehensive Benchmark of Transcriptomic Biomarkers for Immune Checkpoint Blockades. *Cancers (Basel)* **15**, (2023).
35. Sun, S. *et al.* Systematic assessment of transcriptomic biomarkers for immune checkpoint blockade response in cancer immunotherapy. *Cancers (Basel)* **13**, (2021).
36. Hoang, D.-T. *et al.* Path2Omics: Enhanced transcriptomic and methylation prediction accuracy from tumor histopathology. *bioRxiv* Preprint at https://doi.org/10.1101/2025.02.26.640189 (2025).
37. Hoang, D.-T. *et al.* Prediction of cancer treatment response from histopathology images through imputed transcriptomics. *Journal of Clinical Oncology* **41**, (2023).
38. Hoang, D. T. *et al.* A deep-learning framework to predict cancer treatment response from histopathology images through imputed transcriptomics. *Nat Cancer* (2024) doi:10.1038/s43018-024-00793-2.
39. Kalaora, S., Nagler, A., Wargo, J. A. & Samuels, Y. Mechanisms of immune activation and regulation: lessons from melanoma. *Nature Reviews Cancer* vol. 22 Preprint at https://doi.org/10.1038/s41568-022-00442-9 (2022).
40. Yoshihara, K. *et al.* Inferring tumour purity and stromal and immune cell admixture from expression data. *Nat Commun* **4**, (2013).
41. Chen, S. *et al.* Inflammatory response signature score model for predicting immunotherapy response and pan-cancer prognosis. *Comput Struct Biotechnol J* **23**, (2024).
42. Saltz, J. *et al.* Spatial Organization and Molecular Correlation of Tumor-Infiltrating Lymphocytes Using Deep Learning on Pathology Images. *Cell Rep* **23**, (2018).
43. Jerby-Arnon, L. *et al.* A Cancer Cell Program Promotes T Cell Exclusion and Resistance to Checkpoint Blockade. *Cell* **175**, (2018).
44. Foy, J. P. *et al.* Immunologically active phenotype by gene expression profiling is associated with clinical benefit from PD-1/PD-L1 inhibitors in real-world head and neck and lung cancer patients. *Eur J Cancer* **174**, (2022).
45. Thorsson, V. *et al.* The Immune Landscape of Cancer. *Immunity* **48**, (2018).
46. Amgad, M. *et al.* Structured crowdsourcing enables convolutional segmentation of histology images. *Bioinformatics* **35**, (2019).
47. Amgad, M. *et al.* NuCLS: A scalable crowdsourcing approach and dataset for nucleus classification and segmentation in breast cancer. *Gigascience* **11**, (2022).
48. Lee, J. S. & Ruppin, E. Multiomics Prediction of Response Rates to Therapies to Inhibit Programmed Cell Death 1 and Programmed Cell Death 1 Ligand 1. *JAMA Oncol* **5**, (2019).
49. Sinha, N. *et al.* Immune Determinants of the Association between Tumor Mutational Burden and Immunotherapy Response across Cancer Types. *Cancer Res* **82**, (2022).
50. Gide, T. N. *et al.* Distinct Immune Cell Populations Define Response to Anti-PD-1 Monotherapy and Anti-PD-1/Anti-CTLA-4 Combined Therapy. *Cancer Cell* **35**, (2019).
51. Riaz, N. *et al.* Tumor and Microenvironment Evolution during Immunotherapy with Nivolumab. *Cell* **171**, (2017).
52. Keenan, T. E. *et al.* Molecular correlates of response to eribulin and pembrolizumab in hormone receptor-positive metastatic breast cancer. *Nat Commun* **12**, (2021).

53. Shan, N. L. *et al.* Circulating tumor DNA fraction predicts residual cancer burden post-neoadjuvant chemotherapy in triple negative breast cancer. *The Journal of Liquid Biopsy* **6**, 100168 (2024).
54. Motzer, R. J. *et al.* Molecular Subsets in Renal Cancer Determine Outcome to Checkpoint and Angiogenesis Blockade. *Cancer Cell* **38**, (2020).
55. Miao, D. *et al.* Genomic correlates of response to immune checkpoint therapies in clear cell renal cell carcinoma. *Science (1979)* **359**, (2018).
56. Obradovic, A. *et al.* Immunostimulatory Cancer-Associated Fibroblast Subpopulations Can Predict Immunotherapy Response in Head and Neck Cancer. *Clinical Cancer Research* **28**, (2022).
57. Campbell, K. M. *et al.* Oral Cavity Squamous Cell Carcinoma Xenografts Retain Complex Genotypes and Intertumor Molecular Heterogeneity. *Cell Rep* **24**, (2018).
58. Markovits, E. *et al.* MYC Induces Immunotherapy and IFNg Resistance Through Downregulation of JAK2. *Cancer Immunol Res* **11**, (2023).
59. Cui, C. *et al.* Ratio of the interferon-γ signature to the immunosuppression signature predicts anti-PD-1 therapy response in melanoma. *NPJ Genom Med* **6**, (2021).
60. Nair, N. U. *et al.* Genomic and transcriptomic analyses identify a prognostic gene signature and predict response to therapy in pleural and peritoneal mesothelioma. *Cell Rep Med* **4**, (2023).
61. Cho, J. W. *et al.* Genome-wide identification of differentially methylated promoters and enhancers associated with response to anti-PD-1 therapy in non-small cell lung cancer. *Exp Mol Med* **52**, (2020).
62. Kim, J. Y., Choi, J. K. & Jung, H. Genome-wide methylation patterns predict clinical benefit of immunotherapy in lung cancer. *Clin Epigenetics* **12**, (2020).
63. Jung, H. *et al.* DNA methylation loss promotes immune evasion of tumours with high mutation and copy number load. *Nat Commun* **10**, (2019).
64. Ravi, A. *et al.* Genomic and transcriptomic analysis of checkpoint blockade response in advanced non-small cell lung cancer. *Nat Genet* **55**, (2023).
65. Van Allen, E. M. *et al.* Genomic correlates of response to CTLA-4 blockade in metastatic melanoma. *Science (1979)* **350**, (2015).
66. Sidders, B. *et al.* Adenosine Signaling Is Prognostic for Cancer Outcome and Has Predictive Utility for Immunotherapeutic Response. *Clin Cancer Res* **26**, (2020).
67. Shukla, S. A. *et al.* Cancer-Germline Antigen Expression Discriminates Clinical Outcome to CTLA-4 Blockade. *Cell* **173**, (2018).
68. Rooney, M. S., Shukla, S. A., Wu, C. J., Getz, G. & Hacohen, N. Molecular and genetic properties of tumors associated with local immune cytolytic activity. *Cell* **160**, (2015).
69. Wang, L. *et al.* Enhancing KDM5A and TLR activity improves the response to immune checkpoint blockade. *Sci Transl Med* **12**, (2020).
70. Dominguez, C. X. *et al.* Single-cell RNA sequencing reveals stromal evolution into LRRC15+ myofibroblasts as a determinant of patient response to cancer immunotherapy. *Cancer Discov* **10**, (2020).
71. Mariathasan, S. *et al.* TGFβ attenuates tumour response to PD-L1 blockade by contributing to exclusion of T cells. *Nature* **554**, (2018).
72. Xiong, D., Wang, Y. & You, M. A gene expression signature of TREM2hi macrophages and γδ T cells predicts immunotherapy response. *Nat Commun* **11**, (2020).
73. Bareche, Y. *et al.* Leveraging big data of immune checkpoint blockade response identifies novel potential targets. *Annals of Oncology* **33**, (2022).
74. Chang, T. G. *et al.* LORIS robustly predicts patient outcomes with immune checkpoint blockade therapy using common clinical, pathologic and genomic features. *Nat Cancer* **5**, 1158–1175 (2024).
75. Zhang, H. *et al.* Prediction and analysis of tumor infiltrating lymphocytes across 28 cancers by TILScout using deep learning. *NPJ Precis Oncol* **9**, (2025).
76. Shulman, E. D. *et al.* AI-Driven Spatial Transcriptomics Unlocks Large-Scale Breast Cancer Biomarker Discovery from Histopathology. *bioRxiv* Preprint at https://doi.org/10.1101/2024.10.16.618609 (2024).
77. Goldman, M. J. *et al.* Visualizing and interpreting cancer genomics data via the Xena platform. *Nature Biotechnology* vol. 38 Preprint at https://doi.org/10.1038/s41587-020-0546-8 (2020).
78. Schwartz, L. H. *et al.* RECIST 1.1 - Update and clarification: From the RECIST committee. *Eur J Cancer* **62**, (2016).

79. Patro, R., Duggal, G., Love, M. I., Irizarry, R. A. & Kingsford, C. Salmon provides fast and bias-aware quantification of transcript expression. *Nat Methods* **14**, (2017).
80. Soneson, C., Love, M. I. & Robinson, M. D. Differential analyses for RNA-seq: transcript-level estimates improve gene-level inferences. *F1000Res* **4**, (2015).
81. Ritchie, M. E. *et al.* Limma powers differential expression analyses for RNA-sequencing and microarray studies. *Nucleic Acids Res* **43**, (2015).
82. Kuleshov, M. V. *et al.* Enrichr: a comprehensive gene set enrichment analysis web server 2016 update. *Nucleic Acids Res* **44**, (2016).
83. Langfelder, P. & Horvath, S. WGCNA: An R package for weighted correlation network analysis. *BMC Bioinformatics* (2008) doi:10.1186/1471-2105-9-559.
84. Hänzelmann, S., Castelo, R. & Guinney, J. GSVA: Gene set variation analysis for microarray and RNA-Seq data. *BMC Bioinformatics* **14**, (2013).
85. Han, Y. *et al.* TISCH2: expanded datasets and new tools for single-cell transcriptome analyses of the tumor microenvironment. *Nucleic Acids Res* **51**, (2023).
86. Hao, J. & Ho, T. K. Machine Learning Made Easy: A Review of Scikit-learn Package in Python Programming Language. *Journal of Educational and Behavioral Statistics* vol. 44 Preprint at https://doi.org/10.3102/1076998619832248 (2019).
87. Hughes, G. Youden's index and the weight of evidence revisited. *Methods of Information in Medicine* vol. 54 Preprint at https://doi.org/10.3414/ME15-04-0007 (2015).
88. Girardi, D. M. *et al.* Cabozantinib plus Nivolumab Phase I Expansion Study in Patients with Metastatic Urothelial Carcinoma Refractory to Immune Checkpoint Inhibitor Therapy. *Clinical Cancer Research* **28**, (2022).
89. Apolo, A. B. *et al.* Final Results From a Phase I Trial and Expansion Cohorts of Cabozantinib and Nivolumab Alone or With Ipilimumab for Advanced/Metastatic Genitourinary Tumors. *Journal of Clinical Oncology* **42**, 3033–3046 (2024).
90. Atkins, M. B. *et al.* Phase II Study of Nivolumab and Salvage Nivolumab/Ipilimumab in Treatment-Naive Patients with Advanced Clear Cell Renal Cell Carcinoma (HCRN GU16-260-Cohort A). *Journal of Clinical Oncology* **373**, (2022).
91. Atkins, M. B. *et al.* Phase II study of nivolumab and salvage nivolumab/ipilimumab in treatment-naïve patients with advanced non-clear cell renal cell carcinoma (HCRN GU16-260-Cohort B). *J Immunother Cancer* **11**, (2023).
92. El Ahmar, N. *et al.* Biomarkers of response to first-line nivolumab therapy in patients with advanced renal cell carcinoma (RCC) enrolled in the HCRN GU16-260 trial. *Journal of Clinical Oncology* **41**, (2023).
93. Hugaboom, M. B. *et al.* Presence of Tertiary Lymphoid Structures and Exhausted Tissue-Resident T Cells Determines Clinical Response to PD-1 Blockade in Renal Cell Carcinoma. *Cancer Discov* **15**, 948–968 (2025).

(a)

Step 1: TCGA melanoma samples "Hot" and "Cold" immune phenotype classification

TCGA Melanoma

Immune Score

Inflammation Score

Number of TIL patches

Identify tumor samples exhibiting extreme Hot and Cold Tumor Immune Microenvironment (TIME)

Samples	Immune Score	Inflammation Score	Number of TIL patches	Annotated group
Sample 1	Top 30%	Top 30 %	Top 30%	**Hot**
Sample 2	Top 30%	Top 30%	Bottom 30%	-
Sample 3	Top 30%	Middle	Top 30%	**Hot**
Sample 4	Bottom 30%	Bottom 30%	Bottom 30%	**Cold**
Sample 5	Bottom 30%	Bottom 30%	Middle	**Cold**
Sample 5	Bottom 30%	Top 30%	Middle	-

Classify the TCGA melanoma samples based on the top 30 and bottom 30 Percentiles based on these three scores

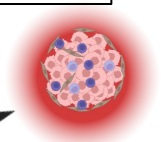

Hot Tumor (Activated TIME)

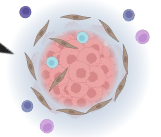

Cold Tumor (Inactivated TIME)

(b)

Step 2: Derivation of Tumor Immune Microenvironment Activation (TIME_ACT) Gene Signature and its application to predict ICB response from patient transcriptomics data

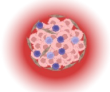

Hot Tumor

Cold Tumor

DEG Analysis

Identified genes that are highly upregulated in hot tumors

Gene-set Enrichment Analysis

Identified those genes that are enriched in immune-related processes

TIME_ACT (Tumor Immune MicroEnvironment ACTivation) Gene Signature

Co-expression Network Analysis

Demonstrated that TIME_ACT genes form a co-expressed, functionally related immune activation module

Pan-cancer Analysis

TIME_ACT scores accurately identify tumor immune activation in other cancer types

scRNA-seq analysis

TIME_ACT genes are predominantly expressed in immune cells and not in malignant cells

Spatial transcriptomics analysis

TIME_ACT-high regions are enriched for lymphocyte infiltration in close proximity to tumor cells

No	Cancer Type	Datasets	Sample Size	ICB Treatment
1	Breast cancer	phs002419	14	anti-PD1
2	Breast cancer	PRJNA558949	50	anti-PD1
3	ccRCC	EGAS00001004353	354	anti-PD1
4	ccRCC	phs001493	29	anti-PD1
5	HNSCC	GSE159067	102	anti-PD1
6	HNSCC	GSE195832	20	anti-PD1
7	HNSCC	phs001623	24	anti-PD1
8	Melanoma	GSE160638	28	anti-PD1
9	Melanoma	GSE91061	49	anti-PD1
10	Melanoma	PRJEB23709	41	anti-PD1
11	Melanoma	PUCH_cohort	55	anti-PD1
12	Melanoma	phs000452.v2.p1	42	anti-CTLA4
13	Mesothelioma	phs002207	16	anti-PD1
14	NSCLC	GSE126044	16	anti-PD1
15	NSCLC	GSE135222	27	anti-PD1
16	NSCLC	phs002822	118	anti-PD1

	Patient 1	Patient 2	...
Gene 1	10.33	5.38	...
Gene 2	11.07	6.38	...
...	...	...	...

	TIME_ACT score
Patient 1	0.46
Patient 2	-0.13
...	...

Predict ICB Response

Responder

Non-Responder

(c)

Step 3: Predicting expression of TIME_ACT genes and ICB treatment response directly from pathology slides

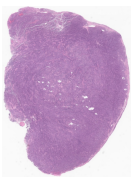

Tumor pathology slide

Path2Omics

No.	Cohort name	Treatment	#Slides	Source
1	NCI-BLCA	ICB	48	NCI *(Unpublished)*
2	Cedars-Sinai SKCM	ICB	35	Cedars-Sinai *(Unpublished)*
3	Cedars-Sinai BRCA	ICB	23	Cedars-Sinai *(Unpublished)*
4	Cedars-Sinai LUAD	ICB	30	Cedars-Sinai *(Unpublished)*
5	HCRN-KIRC	ICB	151	HCRN *(Unpublished)*
6	HCRN-KIRP	ICB	48	HCRN *(Unpublished)*
7	Taiwan-HNSCC$_1$	ICB	33	NYCU Taiwan *(Unpublished)*
8	Taiwan-HNSCC$_2$	ICB	61	NYCU Taiwan *(Unpublished)*
	Total		**429**	

Slide-inferred Gene Expression

	Slide1	Slide2	Slide3
Gene 1	10.33	5.38	2.32
Gene 2	11.07	6.38	8.45
...	...	...	...

	TIME_ACT score
Slide 1	0.46
Slide 2	-0.13
...	...

Predict ICB Response

Responder

Non-Responder

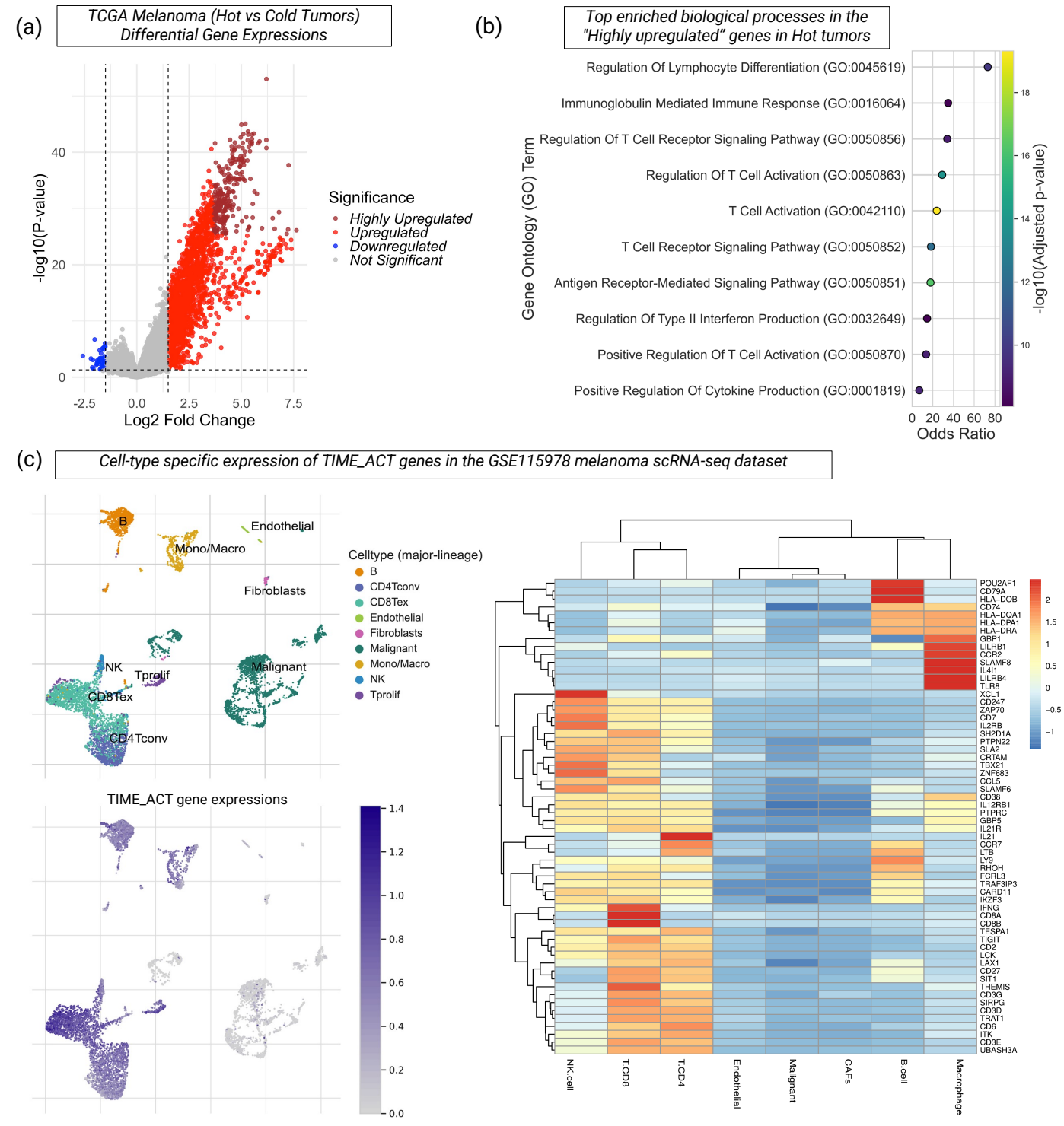
(a)
TCGA Melanoma (Hot vs Cold Tumors)
Differential Gene Expressions
-log10(P-value)
Log2 Fold Change
Significance
Highly Upregulated
Upregulated
Downregulated
Not Significant
(b)
Top enriched biological processes in the "Highly upregulated" genes in Hot tumors
Gene Ontology (GO) Term
Regulation Of Lymphocyte Differentiation (GO:0045619)
Immunoglobulin Mediated Immune Response (GO:0016064)
Regulation Of T Cell Receptor Signaling Pathway (GO:0050856)
Regulation Of T Cell Activation (GO:0050863)
T Cell Activation (GO:0042110)
T Cell Receptor Signaling Pathway (GO:0050852)
Antigen Receptor-Mediated Signaling Pathway (GO:0050851)
Regulation Of Type II Interferon Production (GO:0032649)
Positive Regulation Of T Cell Activation (GO:0050870)
Positive Regulation Of Cytokine Production (GO:0001819)
Odds Ratio
-log10(Adjusted p-value)
(c)
Cell-type specific expression of TIME_ACT genes in the GSE115978 melanoma scRNA-seq dataset
B
Endothelial
Mono/Macro
Fibroblasts
NK
Tprolif
Malignant
CD8Tex
CD4Tconv
Celltype (major-lineage)
B
CD4Tconv
CD8Tex
Endothelial
Fibroblasts
Malignant
Mono/Macro
NK
Tprolif
TIME_ACT gene expressions
NK.cell
T.CD8
T.CD4
Endothelial
Malignant
CAFs
B.cell
Macrophage

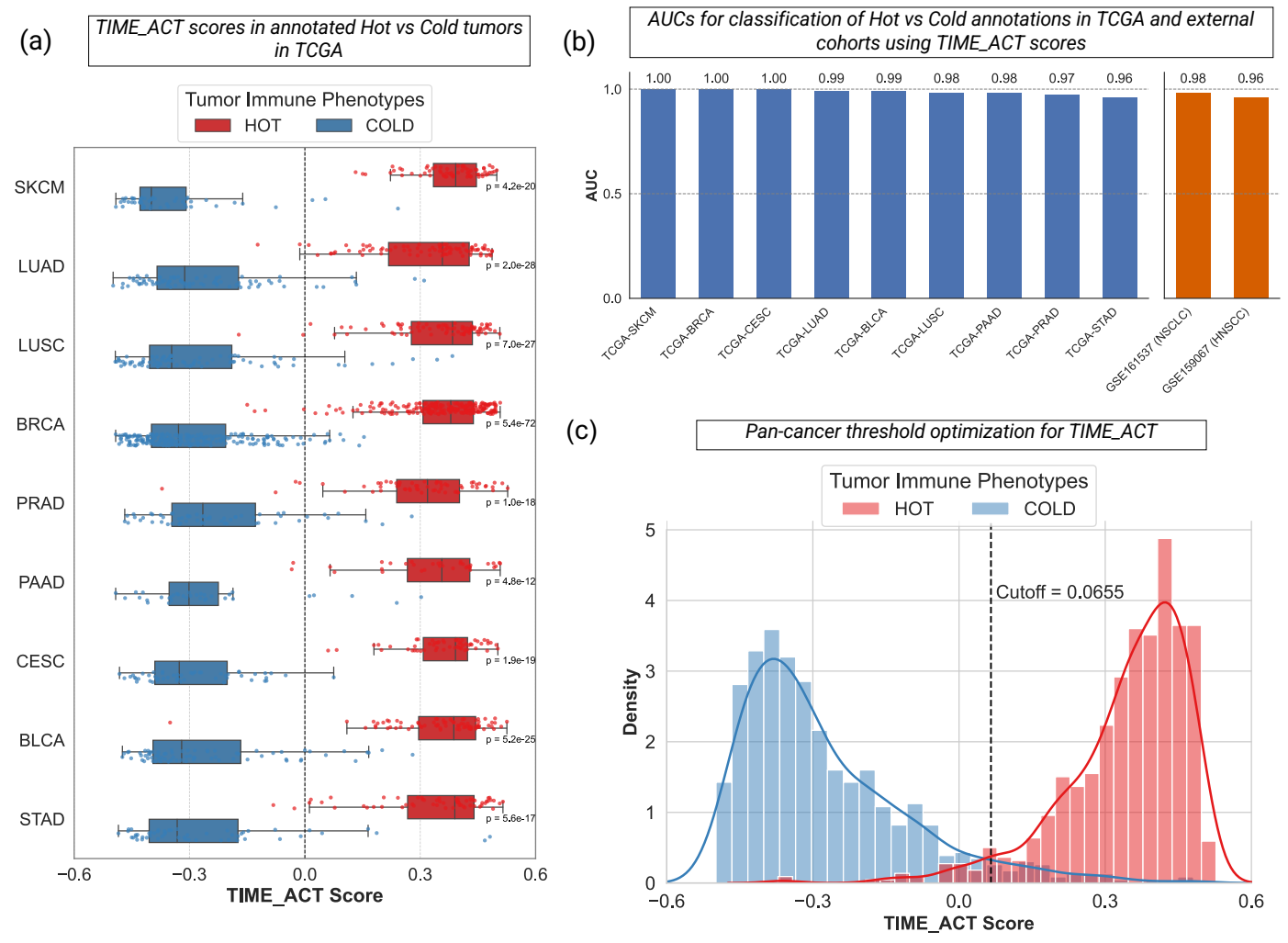
(a)
TIME_ACT scores in annotated Hot vs Cold tumors in TCGA
Tumor Immune Phenotypes
HOT
COLD
SKCM
LUAD
LUSC
BRCA
PRAD
PAAD
CESC
BLCA
STAD
p = 4.2e-20
p = 2.0e-28
p = 7.0e-27
p = 5.4e-72
p = 1.0e-18
p = 4.8e-12
p = 1.9e-19
p = 5.2e-25
p = 5.6e-17
−0.6
−0.3
0.0
0.3
0.6
TIME_ACT Score
(b)
AUCs for classification of Hot vs Cold annotations in TCGA and external cohorts using TIME_ACT scores
AUC
1.0
0.5
0.0
1.00
1.00
1.00
0.99
0.99
0.98
0.98
0.97
0.96
0.98
0.96
TCGA-SKCM
TCGA-BRCA
TCGA-CESC
TCGA-LUAD
TCGA-BLCA
TCGA-LUSC
TCGA-PAAD
TCGA-PRAD
TCGA-STAD
GSE161537 (NSCLC)
GSE159067 (HNSCC)
(c)
Pan-cancer threshold optimization for TIME_ACT
Tumor Immune Phenotypes
HOT
COLD
Cutoff = 0.0655
Density
0
1
2
3
4
5
−0.6
−0.3
0.0
0.3
0.6
TIME_ACT Score

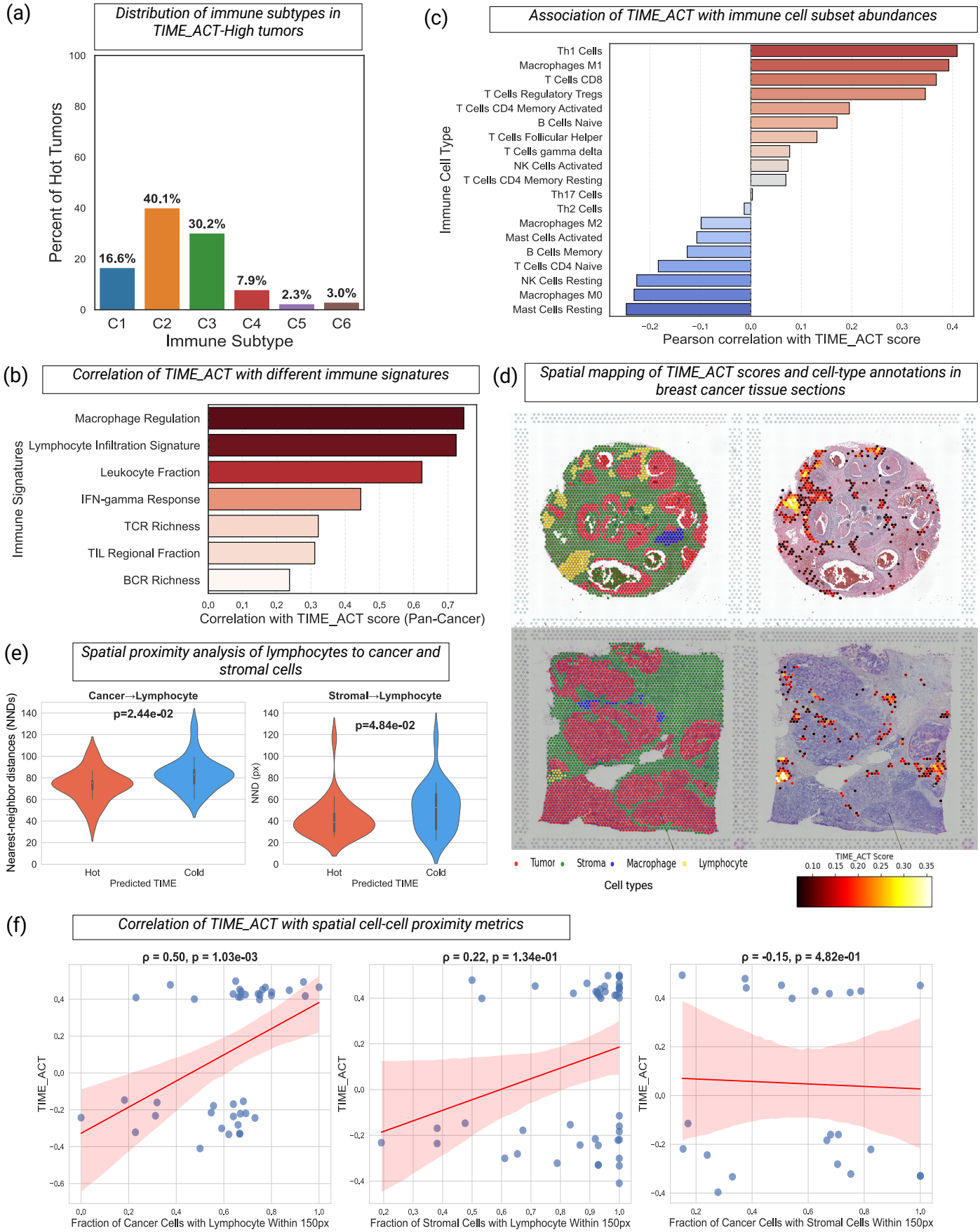
(a)
Distribution of immune subtypes in TIME_ACT-High tumors
Percent of Hot Tumors
Immune Subtype
C1
C2
C3
C4
C5
C6
16.6%
40.1%
30.2%
7.9%
2.3%
3.0%
(c)
Association of TIME_ACT with immune cell subset abundances
Immune Cell Type
Th1 Cells
Macrophages M1
T Cells CD8
T Cells Regulatory Tregs
T Cells CD4 Memory Activated
B Cells Naive
T Cells Follicular Helper
T Cells gamma delta
NK Cells Activated
T Cells CD4 Memory Resting
Th17 Cells
Th2 Cells
Macrophages M2
Mast Cells Activated
B Cells Memory
T Cells CD4 Naive
NK Cells Resting
Macrophages M0
Mast Cells Resting
Pearson correlation with TIME_ACT score
(b)
Correlation of TIME_ACT with different immune signatures
Immune Signatures
Macrophage Regulation
Lymphocyte Infiltration Signature
Leukocyte Fraction
IFN-gamma Response
TCR Richness
TIL Regional Fraction
BCR Richness
Correlation with TIME_ACT score (Pan-Cancer)
(d)
Spatial mapping of TIME_ACT scores and cell-type annotations in breast cancer tissue sections
Tumor
Stroma
Macrophage
Lymphocyte
Cell types
TIME_ACT Score
(e)
Spatial proximity analysis of lymphocytes to cancer and stromal cells
Cancer→Lymphocyte
p=2.44e-02
Stromal→Lymphocyte
p=4.84e-02
Nearest-neighbor distances (NNDs)
NND (px)
Hot
Cold
Predicted TIME
(f)
Correlation of TIME_ACT with spatial cell-cell proximity metrics
ρ = 0.50, p = 1.03e-03
ρ = 0.22, p = 1.34e-01
ρ = -0.15, p = 4.82e-01
TIME_ACT
Fraction of Cancer Cells with Lymphocyte Within 150px
Fraction of Stromal Cells with Lymphocyte Within 150px
Fraction of Cancer Cells with Stromal Cells Within 150px

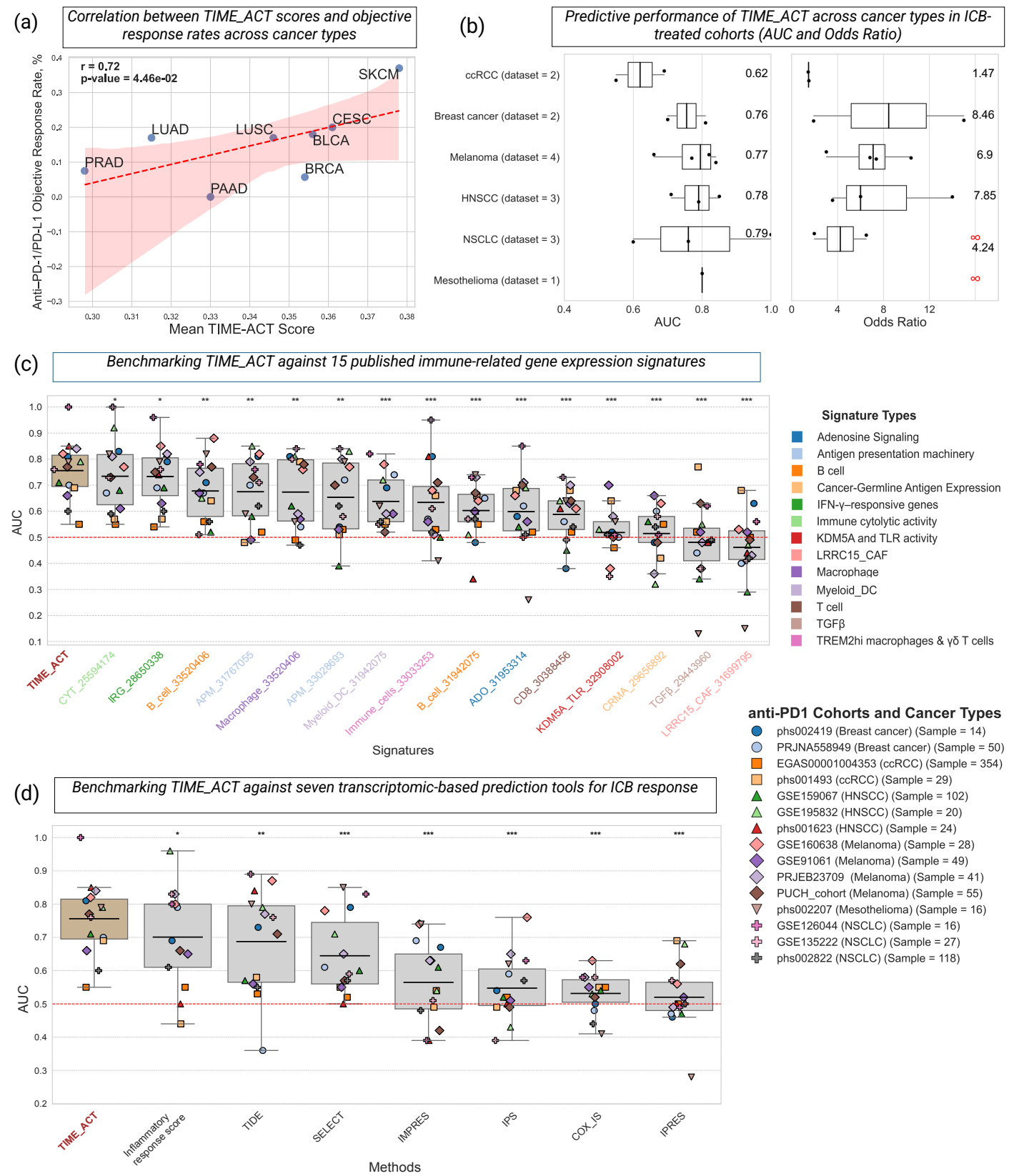
(a)
Correlation between TIME_ACT scores and objective response rates across cancer types
r = 0.72
p-value = 4.46e-02
SKCM
LUAD
LUSC
CESC
BLCA
PRAD
BRCA
PAAD
Anti–PD-1/PD-L1 Objective Response Rate, %
Mean TIME-ACT Score
(b)
Predictive performance of TIME_ACT across cancer types in ICB-treated cohorts (AUC and Odds Ratio)
ccRCC (dataset = 2)
Breast cancer (dataset = 2)
Melanoma (dataset = 4)
HNSCC (dataset = 3)
NSCLC (dataset = 3)
Mesothelioma (dataset = 1)
0.62
0.76
0.77
0.78
0.79
1.47
8.46
6.9
7.85
∞
4.24
∞
AUC
Odds Ratio
(c)
Benchmarking TIME_ACT against 15 published immune-related gene expression signatures
AUC
TIME_ACT
CYT_25594174
IRG_28650338
B_cell_33520406
APM_31767055
Macrophage_33520406
APM_33028693
Myeloid_DC_31942075
Immune_cells_33033253
B_cell_31942075
ADO_31953314
CD8_30388456
KDM5A_TLR_32908002
CRMA_29656892
TGFβ_29443960
LRRC15_CAF_31699795
Signatures
Signature Types
Adenosine Signaling
Antigen presentation machinery
B cell
Cancer-Germline Antigen Expression
IFN-γ–responsive genes
Immune cytolytic activity
KDM5A and TLR activity
LRRC15_CAF
Macrophage
Myeloid_DC
T cell
TGFβ
TREM2hi macrophages & γδ T cells
anti-PD1 Cohorts and Cancer Types
phs002419 (Breast cancer) (Sample = 14)
PRJNA558949 (Breast cancer) (Sample = 50)
EGAS00001004353 (ccRCC) (Sample = 354)
phs001493 (ccRCC) (Sample = 29)
GSE159067 (HNSCC) (Sample = 102)
GSE195832 (HNSCC) (Sample = 20)
phs001623 (HNSCC) (Sample = 24)
GSE160638 (Melanoma) (Sample = 28)
GSE91061 (Melanoma) (Sample = 49)
PRJEB23709 (Melanoma) (Sample = 41)
PUCH_cohort (Melanoma) (Sample = 55)
phs002207 (Mesothelioma) (Sample = 16)
GSE126044 (NSCLC) (Sample = 16)
GSE135222 (NSCLC) (Sample = 27)
phs002822 (NSCLC) (Sample = 118)
(d)
Benchmarking TIME_ACT against seven transcriptomic-based prediction tools for ICB response
AUC
TIME_ACT
Inflammatory response score
TIDE
SELECT
IMPRES
IPS
COX_IS
IPRES
Methods

(a)

Correlation of slide-inferred vs actual expression for TIME_ACT genes compared to all genes across TCGA cancer types

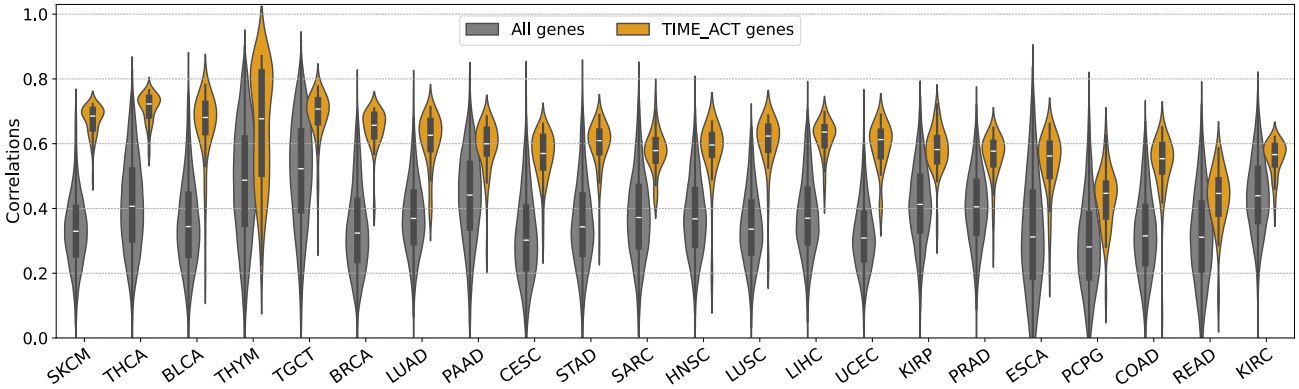

(b)

Comparison of AUCs for Hot vs Cold classification using measured vs slide-inferred TIME_ACT scores across TCGA cancers

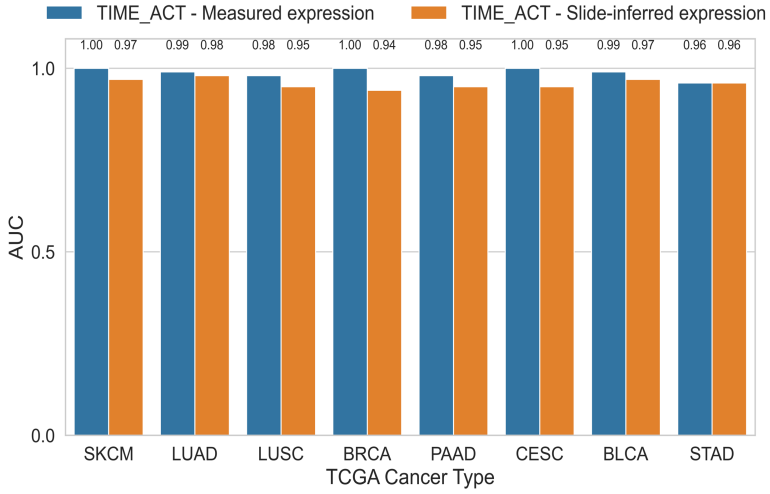

(c)

Prediction performance (AUC and Odds Ratio) of slide-inferred TIME_ACT in eight new ICB clinical cohorts

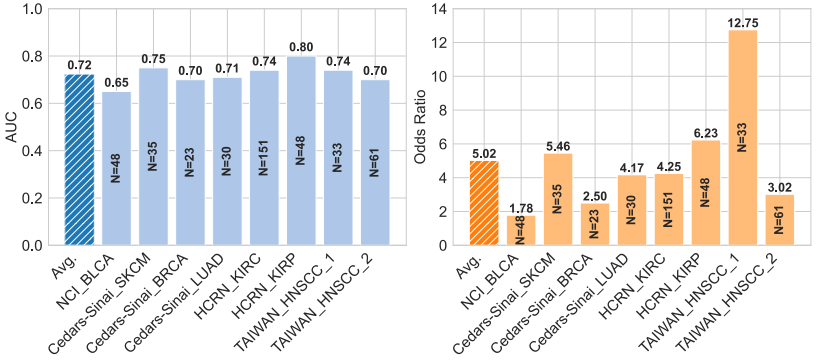

(d)

Comparison of slide-inferred vs measured TIME_ACT scores in matched cohorts

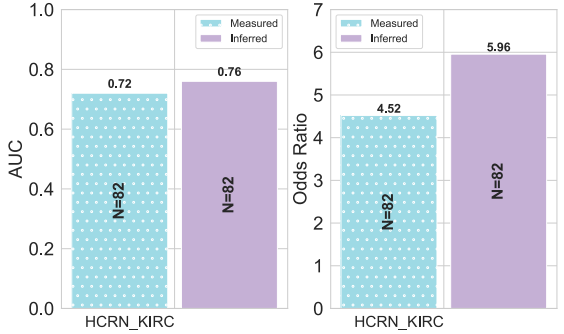

(e)
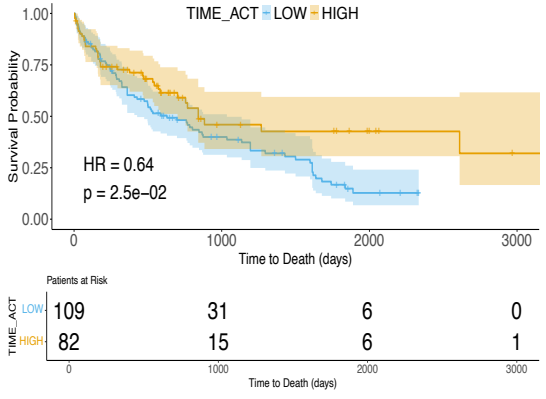
Survival analysis in ICB-treated LUAD patients (Sheba Cohort) stratified by slide-inferred TIME_ACT score